NUMERICAL INVESTIGATION OF FLOW CONTROL OVER AN AIRFOIL WITH SYNTHETIC JETS AND ITS OPTIMIZATION

A THESIS SUBMITTED TO
THE GRADUATE SCHOOL OF NATURAL AND APPLIED SCIENCES
OF
MIDDLE EAST TECHNICAL UNIVERSITY

BY

ERAY AKÇAYÖZ

IN PARTIAL FULFILLMENT OF THE REQUIREMENTS
FOR
THE DEGREE OF MASTER OF SCIENCE
IN
AEROSPACE ENGINEERING

SEPTEMBER 2008

Approval of the thesis:

NUMERICAL INVESTIGATION OF FLOW CONTROL OVER AN AIRFOIL WITH SYNTHETIC JETS AND ITS OPTIMIZATION

submitted by **ERAY AKÇAYÖZ** in partial fulfillment of the requirements for the degree of **Master of Science in Aerospace Engineering Department, Middle East Technical University** by,

Prof. Dr. Canan Özgen
Dean, Gradute School of **Natural and Applied Sciences** _____

Prof. Dr. İsmail H. Tuncer
Head of Department, **Aerospace Engineering** _____

Prof. Dr. İsmail H. Tuncer
Supervisor, **Aerospace Engineering Dept., METU** _____

Examining Committee Members:

Prof. Dr. Cahit Çıray
Aerospace Engineering Dept., METU _____

Prof. Dr. İsmail H. Tuncer
Aerospace Engineering Dept., METU _____

Prof. Dr. M. Haluk Aksel
Mechanical Engineering Dept., METU _____

Assist. Prof. Dr. Oğuz Uzol
Aerospace Engineering Dept., METU _____

Dr. Sartuk Karasoy
Manager, ROKETSAN A.Ş. _____

Date: _____

I hereby declare that all information in this document has been obtained and presented in accordance with academic rules and ethical conduct. I also declare that, as required by these rules and conduct, I have fully cited and referenced all material and results that are not original to this work.

Name, Last Name: Eray Akçayöz

Signature :

ABSTRACT

NUMERICAL INVESTIGATION OF FLOW CONTROL
OVER AN AIRFOIL WITH SYNTHETIC JETS AND ITS OPTIMIZATION

Akçayöz, Eray
M.S., Department of Aerospace Engineering
Supervisor : Prof. Dr. İsmail H. Tuncer

September 2008, 73 pages

In this work, an active flow control method is studied numerically by using a synthetic jet over a NACA 0015 airfoil. Unsteady, turbulent flows over the NACA 0015 airfoil are computed using a Navier-Stokes solver. The Spalart-Allmaras turbulence model is employed in all computations. Unsteady flow solutions are computed in parallel using Parallel Virtual Machine library routines in a computer cluster. The synthetic jet is implemented to the flow solver as a boundary condition. Response Surface Methodology is employed for the optimization of synthetic jet parameters at various angles of attack. The synthetic jet parameters; the jet velocity, the jet location, the jet angle and the jet frequency are optimized to maximize the lift to drag ratio. The optimization study is performed for a constant value of jet power coefficient. The jet slot size is used as a dependent parameter in the optimization studies.

The optimization study has shown that the jet velocity and the jet location are the dominant synthetic jet parameters. The optimum synthetic jet angle is observed to be increasing as the angle of attack increases. The optimum jet location is observed to be moving through the leading edge as angle of attack increases for the separated flows. It is observed that the

application of the synthetic jet delays the flow separation on the suction side of the airfoil and increases the lift to drag ratio significantly especially at post stall angles of attack. The application of the synthetic jet is observed to be less effective for attached flows.

Keywords: Flow Control, Synthetic Jets, Optimization, Parallel Processing, Response Surface Methodology

ÖZ

KANAT KESİDİ ÜZERİNE YERLEŞTİRİLEN
SENTETİK JETİN SAYISAL OLARAK İNCELENMESİ VE OPTİMİZASYONU

Akçayöz, Eray
Yüksek Lisans, Havacılık ve Uzay Mühendisliği Bölümü
Tez Yöneticisi : Prof. Dr. İsmail H. Tuncer

Eylül 2008, 73 sayfa

Bu çalışmada, NACA 0015 kanat kesidi üzerine sentetik jet uygulanarak aktif akış kontrolü sayısal olarak incelenmiştir. NACA 0015 kanat kesidi üzerinde oluşan zamana bağlı, türbülanslı akış Navier-Stokes akış çözücü kullanılarak hesaplanmıştır. Tüm hesaplamalarda Spalart-Allmaras türbülans modeli kullanılmıştır. Zamana bağlı akış hesaplamaları, Parallel Virtual Machine kütüphanesi kullanılarak paralel olarak yapılmıştır. Sentetik jet, Navier-Stokes akış çözücüsüne bir sınır koşulu olarak eklenmiştir. Eniyileştirme çalışmalarında, sentetik jete ait parametrelerin eniyileştirilmesi sağlanarak kaldırma ve sürüklenme katsayıları oranının maksimum değeri alması hedeflenmiştir. Sentetik jet parametrelerinin farklı hücum açılarında eniyileştirilmesi için Yanıt Yüzey Yöntemi kullanılmıştır. Kaldırma ve sürüklenme katsayıları oranı sentetik jetin hızı, konumu, açısı ve frekansı kullanılarak eniyileştirilmiştir. Eniyileştirme çalışmaları jet güç katsayısının değeri sabit tutularak gerçekleştirilmiştir. Jet çıkışının genişliği bağımlı bir parametre olarak kullanılmıştır.

Eniyileştirme çalışmalarında, sentetik jetin hızı ve konumunun diğer jet parametrelerine göre daha baskın olduğu görülmüştür. En uygun sentetik jet açısının hücum açısı arttıkça arttığı

gözlemlenmiştir. Akış ayrılmasının olduğu durumlarda, en uygun sentetik jet konumunun hücum açısı arttıkça kanat hücum kenarına kaydığı görülmüştür. Eniyileştirme çalışmaları, kanat üzerine uygulanan sentetik jetin özellikle perdövites açısından büyük hücum açılarında akış ayrılmasını geciktirdiğini ve kaldırma ve sürüklenme katsayıları oranını önemli ölçüde arttırdığını göstermiştir. Kanat üzerindeki akışın yüzeye yapışık olduğu durumlarda sentetik jetin daha az etkili olduğu gözlemlenmiştir.

Anahtar Kelimeler: Akış Kontrölü, Sentetik Jet, Eniyileştirme, Paralel Çözüm, Yanıt Yüzey Yöntemi

To my marvelous family

ACKNOWLEDGMENTS

I would like to thank my supervisor, Prof. Dr. İsmail H. Tuncer for his great care and guidance throughout my studies.

I would like to thank all jury members for their advices and corrections.

I would also like to thank Engin Erler, for her endless friendship and support.

For his assistance, I am grateful to thank Dr. Mustafa Kaya. Thank you for your support and help without concerning any time limitation.

I want to state my thanks to Hakan Tiftikçi for reviewing my thesis and answering all of my questions.

I also want to state my thanks to Yeşim Kubilay for her english corrections.

Thanks to METU, Aerospace Engineering Department for providing me a parallel computing environment.

I finally would like to thank anyone who have supported my thesis effort in any way.

TABLE OF CONTENTS

LIST OF TABLES

TABLES

LIST OF FIGURES

FIGURES

LIST OF ABBREVIATIONS

ROMAN SYMBOLS

a	Speed of sound
BB	Box-Behnken
c	Airfoil chord length
CFD	Computational Fluid Dynamics
C_d	Drag coefficient
C_l	Lift coefficient
C_μ	Jet momentum coefficient
C_p	Pressure coefficient
C_P	Jet power coefficient
DoE	Design of Experiment
DNS	Direct Numerical Simulation
e	Energy
F	Frequency
FF	Full-Factorial
LES	Large Eddy Simulation
L/D	Lift to Drag ratio
M	Mach number
p	Static pressure
PVM	Parallel Virtual Machine
$PLIF$	Planar Laser Induced Fluorescence
$RANS$	Reynolds Averaged Navier Stokes
Re	Reynolds number
RSM	Response Surface Methodology
t	Time
u	Velocity component in ξ direction
UAV	Unmanned Air Vehicles
w	Velocity component in η direction
x	Cartesian spatial coordinate for stream-wise direction
y^+	Non-dimensional wall distance
z	Cartesian spatial coordinate for trans-verse direction
$ZNMF$	Zero Net Mass Flux

GREEK SYMBOLS

α	Angle of attack
γ	Specific heat ratio
η	Curvilinear spatial coordinate for grid in normal direction
μ	Dynamic viscosity
ν	Kinematic viscosity
ρ	Density
ξ	Curvilinear spatial coordinate for grid in circumferential direction

SUBSCRIPTS

∞	Freestream values
jet	Synthetic jet values

SUPERSCRIPTS

$*$	Dimensional parameters

CHAPTER 1

INTRODUCTION

1.1 Introduction

Flow control used to manipulate the flowfield over an aerodynamic body using various techniques. The aim of the flow control can be to prevent/provoke separation, suppress/enhance turbulence or delay/advance transition to obtain benefits in the fields of Lift to Drag ratio (L/D) enhancement, drag reduction, lift enhancement, mixing augmentation and flow induced noise suppression [6]. The science of the flow control dates back to Prandtl [7, 6]. In 1904, he has presented an eight-page paper about boundary-layer. In this paper, he introduced the concept of the boundary-layer, explained the physics behind the flow separation and demonstrated some experimental results where the boundary layer was controlled by applying a blowing jet around a circular cylinder to delay flow separation [8, 9, 6].

After Prandtl's work, the physics underlying the boundary-layer was understood much better. However, the boundary-layer separation is still a major concern in the aviation industry since it entails great energy losses and limits the aerodynamic performance of an aircraft. It causes several problems not only on the design but also on the operation of the designed aircraft. Thus, the control of boundary layer is still a major task for the aerodynamicists. Geometrical shaping, turbulators, slots and slats are the most commonly used techniques to delay the separation. Active flow control is a new phenomenon for today and it is limited to military applications using steady jets because of the complexity of the steady jet systems and large power requirements [10, 11, 12].

A transport aircraft is designed primarily for cruise flight. However, an extra lift is required during takeoff and landing. Control surfaces such as flaps, ailerons generate extra lift but they

also generate extra drag and cause large energy losses. Today, almost all conventional and military aircraft use passive flow control where the control surfaces are employed to control the flow over wings. Here, the word passive means that the flow control is applied only by deflecting the control surfaces and no energy is added to the flow [8]. At high incidence, the effectiveness of the control surfaces decreases due to flow separation which may cause hazardous results. Current research indicates that the active flow control approach gives the opportunity of controlling the flow without decreasing the aerodynamic efficiency.

1.2 Active Flow Control

Flow control on a lifting device, either passive or active, aims to modify the flow such that it behaves in a different manner compared to no control and essentially increases the off-design envelope or the ability of wing to function at extreme attitudes [2]. Active flow control has the ability to change the lift coefficient without changing the angle of attack or deflecting the control surfaces. Here, the word active implies the addition of energy to the flow [13]. Steady suction or blowing and periodic suction or blowing are some of the active flow control techniques that have been used in past studies. These methods change the shape of the airfoil virtually and have the potential to avoid the flow separation. Suction or blowing type actuators require large amount of power, large space and they are mechanically complex, making them practically difficult to implement [14, 15].

Recently, a better method of active flow control called synthetic jet has been introduced. The synthetic jet is also called Zero Net Mass Flux (ZNMF) jet since it is created by oscillating the fluid around the airfoil periodically. The net mass flux is zero due to periodic sucking and blowing of the air surrounding jet orifice. The synthetic jet induces zero net mass flux however it generates momentum that changes the behavior of the flow. The synthetic jet is created by driving one side of the cavity in a periodic manner. Periodic motion can be generated using electromagnetically driven pistons, acoustically driven cavities or piezoelectrically driven diaphragms [16]. Thus it does not require extra fluid since the fluid around the airfoil is driven mechanically or using electric power. The synthetic jet creates an oscillatory periodic flow that is sucked or blown through an orifice. Figure 1.1 illustrates the sketch of a synthetic jet actuator. In suction phase the fluid is drawn into the cavity and in the blowing phase the fluid is driven out of the cavity and forms a vortex pair. As the vortex pair moves away from the

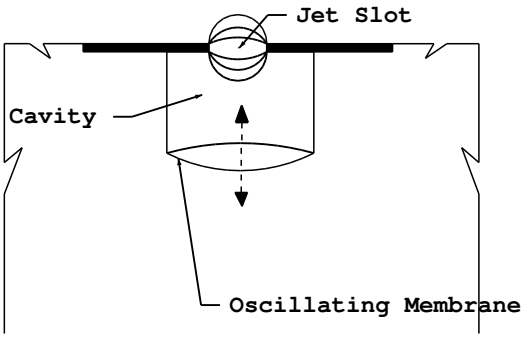

Figure 1.1: Schematic representation of the synthetic jet actuator

orifice, the diaphragm sucks the fluid into the cavity and in the blowing phase, a new vortex pair is created. The generated vortex pairs interact with the separated flow region and causes low pressure region in the interaction zone. The low pressure region around the synthetic jet causes partial or complete reattachment of the flow. Reattachment of the separated flow is responsible from the reduction in pressure drag [17].

The active flow control using synthetic jet is currently becoming an active research field because of its advantages compared with the conventional flow control obtained using lifting surfaces such as flaps, slats etc. [5]. Effectiveness of the conventional control decreases as the angle of attack increases. However, the synthetic jet changes the shape of the airfoil virtually and it can be used at high angles of attack to partially or completely reattach the separated flow. Very large control forces can be generated using active flow control devices that are small in size, light weight and mechanically less complex compared to conventional control devices [14]. Not only does the synthetic jet prevent the flow separation, but it also has a stabilizing effect tending to delay the transition of a laminar boundary layer to a turbulent one [18]. If the active flow control technique could be used effectively, there would be no need to use the conventional control surfaces which cause significant weight penalty [5].

The improvements that can lead to drag reduction is very important if one considers that 1% saving in world consumption of jet fuel is worth about $1.25 millions a day [19]. Recent experimental and computational studies show that if the synthetic jet is applied properly, the

aerodynamic performance of airfoils can be increased in terms of lift enhancement and drag reduction [20, 11, 12, 13].

The active flow control methods can also be used in transition delay, separation postponement, turbulence augmentation and noise suppression [20, 21, 15]. However these effects are not independent from each other. For example, if boundary layer becomes turbulent, resistance to separation increases and more lift can be obtained at high incidence. If transition is delayed, skin friction drag decreases however flow separates easily and increase in form drag occurs. Once the laminar boundary layer separates, a free-shear layer forms and transition to turbulence takes place at high Reynolds numbers. Increased entrainment of high-speed flow due to the turbulent mixing may cause reattachment of the separated region and formation of a laminar separation bubble. At high incidence, the bubble breaks down either by a complete separation or a longer bubble. In both cases, form drag increases and causes a reduction in the lift-curve's slope [7]. All these physical phenomena should considered together which makes the active flow control approach very complex. That's why active flow control is sometimes called as the art of flow control [19].

Understanding the physics behind the synthetic jet interaction with the flow over an airfoil requires a lot of experiments over a wide range of parameters which would be expensive in terms of money and effort. Using a numerical simulation is complementary to experimental investigation. Numerical simulation is more affordable, practical, and systematic therefore it can provide a wider understanding inside the control mechanisms and can lead to the discovery of critical fluid phenomena and pattern changes [22].

1.3 Literature Survey

There are numerous studies in active flow control field especially in the last decade. However, the use of active flow control in industrial aircraft design is still very limited. Recent experimental and computational studies carried out for flow control investigated the effect of synthetic jet on the flow over airfoils.

There are many studies that only concern the behavior of synthetic jet. In the study of Utturkar et al. [23], numerical simulations are performed to define the velocity profiles of two-dimensional and axisymmetric synthetic jets. Lee and Goldstein [1] have performed Direct

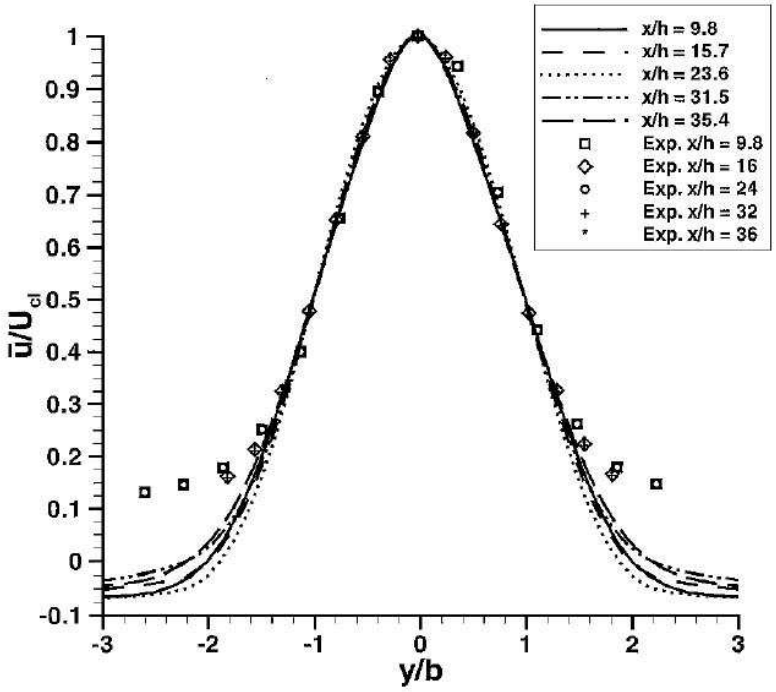

Figure 1.2: Mean velocity variation at various distances from the orifice [1]

Numerical Simulation (DNS) solutions to model synthetic jets. The results of the numerical study are compared with the experimental data of Smith [24]. The plot of streamwise mean velocities at various spanwise distances are shown in Figure 1.2. It is shown that the velocity profile is well predicted along the jet slot except corners.

In the study of Mallinson et al. [15], the flow produced using a synthetic jet has been investigated. It is seen that flow over an airfoil with a synthetic jet becomes periodic more rapidly than the flow over an airfoil with a steady jet. It is reported that rapid establishment of synthetic jet is caused by turbulent dissipation, which keeps a vortex near the orifice, thus limiting the size of the turbulent core.

In the study of Lance et al. [2], an experimental study is performed to evaluate the effectiveness of a synthetic jet actuator for the flow control on a pitching airfoil. The test model is shown in Figure 1.3. The exit slot area is dynamically adjustable and the exit slot of the plenum is curved such that the jet is tangential to the surface, taking the advantage of the Coanda effect. The synthetic jet actuation parameters included the jet momentum coefficient and the slot exit width. In all experiments, the airfoil was pitched from 0^o to 27^o at a constant

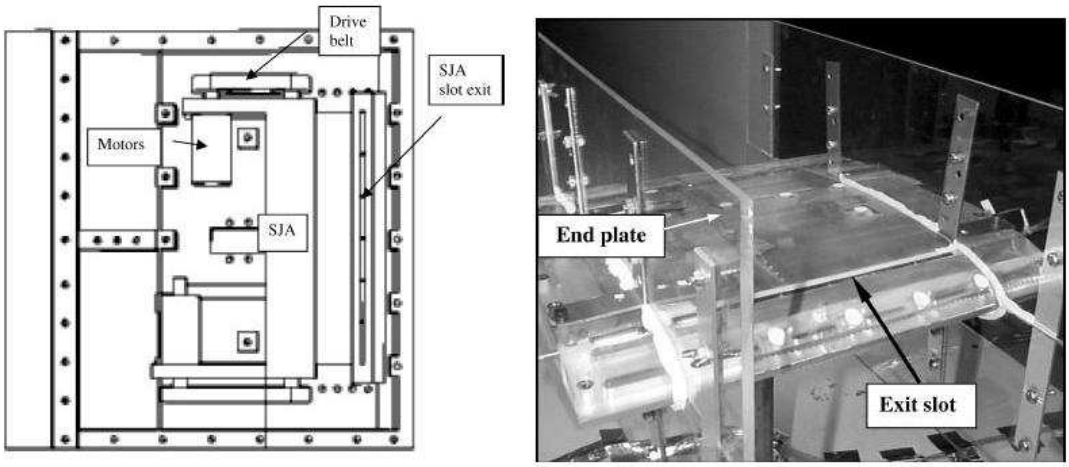

Figure 1.3: Wind tunnel model details and assembled airfoil [2]

angular velocity in 1 second. The results of the experiment have shown that synthetic jet actuation delays the formation of the dynamic-stall-vortex to higher incidence angles.

Hamdani et al. [25] have studied the flow over NACA 0018 when alternating tangential blowing/suction is applied. The active flow control is found to be ineffective for attached flows. Suction is found to be more effective than blowing. During suction, the boundary-layer profile is fuller both at the upstream and downstream of the slot. This is the reason behind the variation in the force coefficients during alternating between blowing and suction jet-applied airfoils. In that study, the jet location is varied and the effectiveness of the jet at these locations is investigated. It is observed that when the jet slot is located before 75% of the chord, the control is effective and the flow separation is suppressed. However, the flow control becomes ineffective when the slot is located at 0.75c which is at the downstream of the separation point. Therefore, it is reported that the slot location is very important parameter for separation control.

Seifert et al. [10] have tested different multi-element airfoils using an oscillatory blowing jet in order to prevent separation that occurs at increasing incidence. The purpose of the flow control is to determine the most important jet parameters affecting the performance of the airfoil. They have shown that when the flow separates from the flap, not from the main body, the blowing from the shoulder of a deflected flap is much more effective than blowing

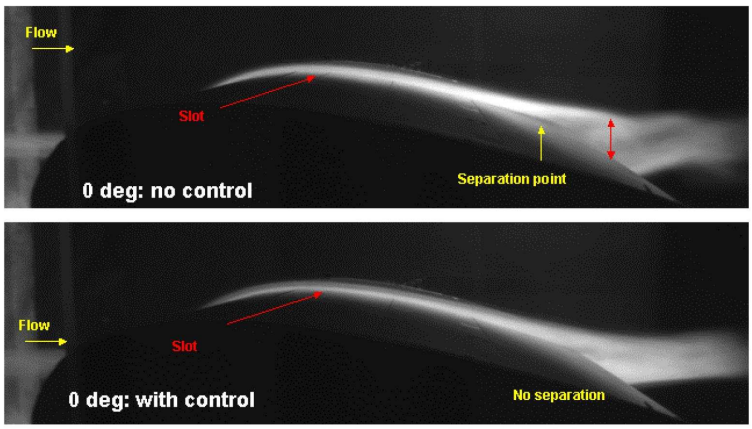

(a) $\alpha = 0^{\circ}$

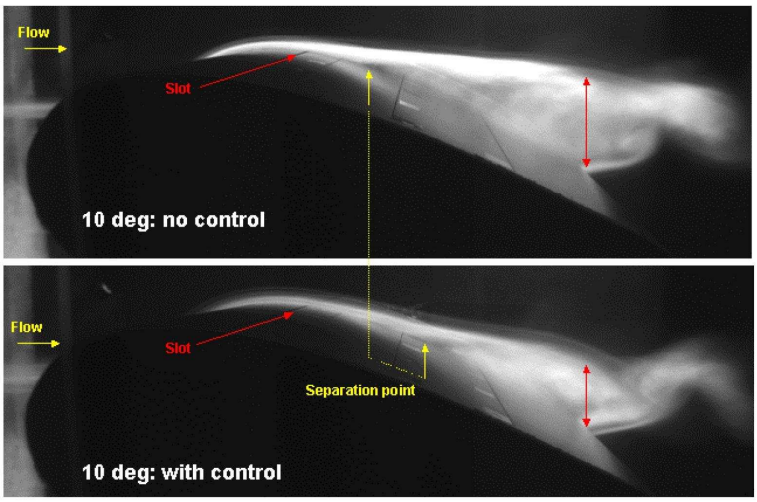

(b) $\alpha = 10^{\circ}$

Figure 1.4: Smoke visualizations with/without flow control [3]

from the leading edge. According to that study, application of oscillatory blowing jet can be used instead of a conventional control since the present method requires low power and its mechanical installation is relatively simple compared to steady suction jets.

Study performed by Martin et al. [3] aims to decrease helicopter pylon/fuselage drag by active flow control. For that purpose, a thick airfoil, NACA 0036 is chosen as baseline 2D test geometry. As can be seen from the flow visualization images shown in Figure 1.4, flow separates even at 0^o angle of attack. Separation is much more severe at 10^o angle of attack. When the flow control is applied, the displacement thickness of the separated shear layer was reduced, but still, a separated bubble is observed near the trailing edge. The effect of the flow control is much more clear at 0^o angle of attack case.

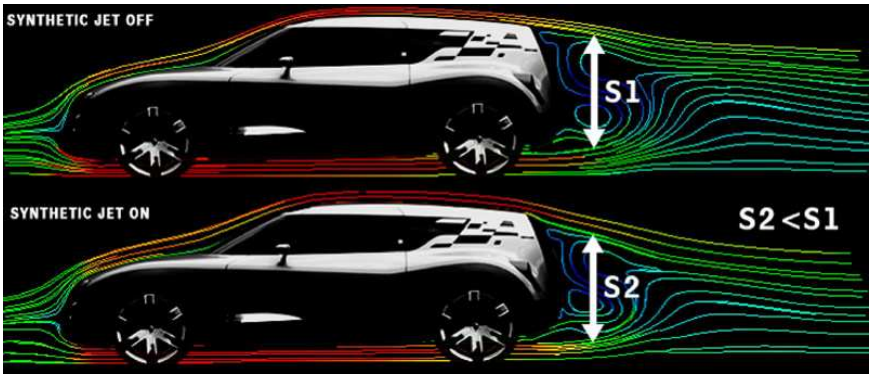

Figure 1.5: Flowfield over the vehicle with synthetic jet is off/on [4]

One of the recent research is the application of the synthetic jet on a Unmanned Air Vehicles, UAV. Parekh et al. [26] have applied the synthetic jet concept over the wings of a UAV. It is reported that the turn rate was increased by controlling the leading edge separation and the weight of the flight control system was reduced. Patel et al. [14] point out that as the synthetic jet technology improves, active flow control can be used in the development of UAVs without conventional control surfaces with a purpose of increasing maneuverability, reducing the observability and weight.

The synthetic jet is implemented in a concept car named as Renault-Altica. The synthetic jet is located at the edge of the rear roof at the point where the flow separates from the vehicle. A discreet mechanical system generates jets of air which are alternately blown and sucked through a 2mm wide slot. The structure of the flow over the edge of the roof is controlled and it is reported that the drag is reduced by 15% at 130 kph with an energy consumption of just 10 Watts. Figure 1.5 shows the flowfield over the vehicle. It is shown the thickness of the separated flow region at the base of the car decreases when the synthetic jet is applied [4].

The Aircraft Morphing program at NASA Langley aims to design an aircraft without conventional control surfaces. Instead of controlling the aircraft using control surfaces, thrust vectoring, adaptive micro-machined surface effectors and distributed devices are planned to be used in the control of an aircraft under different flight conditions. As a part of this program, a NACA 0015 profile is tested in a wind tunnel experiment. The two-dimensional NACA 0015 model which has the dimensions of 91.4 cm span and 91.4 cm chord is shown in Figure 1.6. There are six locations over the model for the installation of the synthetic jet. Experimental

results have shown that, the effect of the synthetic jet reduces when the actuation is applied under the separated flow region. The stagnation line shifts when the actuation is applied near the leading edge such that it changes the overall lift as a similar effect caused by a small angle of attack [5].

Vadillo [17] has made a numerical study on a 24% thick Clark-Y airfoil by employing a synthetic jet. He has observed that the maximum drag reduction with the minimum lift change is observed at higher frequencies of the synthetic jet.

In the numerical study of Wang et al. [27], the active flow control approach is applied to an NACA 63_3-018 airfoil at a stall angle of attack. The influence of jet frequency, intensity and location are investigated. It is found that, the most effective excitation frequency is 1.5 to 2 times of the natural frequency (U_∞/c). The synthetic jet is less effective when it is located at downstream of the natural separation point. The effect of excitation on lift and drag reduces when the jet is excited at a lower intensity since the local pressure field is influenced less.

Numerical investigation of the active flow control using steady and synthetic jets over NACA 0012 and NACA 0015 airfoils is undertaken by Donovan et al. [13]. Navier-Stokes computations are performed using Spalart-Allmaras and SST turbulence models and comparison is made with the experimental data. They have reported that both models show very good agreement before the stall, but deviate from the experimental data after the stall in the uncontrolled case. For the controlled case, the computational results are not in exact agreement with the experiment but they approximate the general trend. It is also reported that in order to get same post-stall lift enhancement obtained with oscillatory jet, a steady jet with one to two orders of magnitude larger blowing momentum coefficient is required. It is observed that for attached flow, actuators change the aerodynamic shape by virtually changing the camber. For separated flow, the primary benefit of the actuator is reported to be reattachment of the separated flow partially. The studies over NACA 0012 airfoil showed that the actuators placed near the leading edge had a stronger effect than the actuators placed farther aft.

Huang et al. [22] have performed a numerical simulation using suction and blowing control over a NACA 0012 airfoil at a Reynolds number of 5.10^5 and at an angle of attack of 18^o. They have changed three jet parameters; jet location, amplitude and angle. They have observed that suction has the advantage of creating a lower pressure on larger area over the upper surface of the airfoil hence, the flow is more attached, lift is enhanced and the profile drag is reduced.

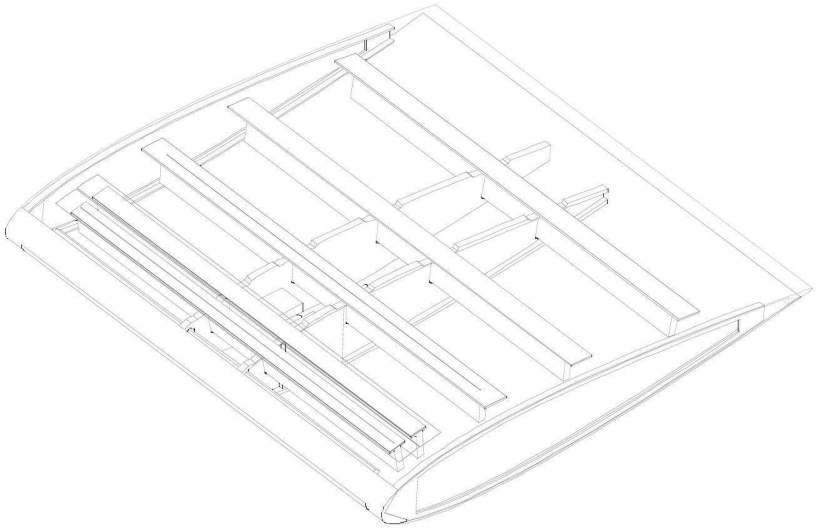

(a) Cut-away view of the airfoil model

(b) Photograph of airfoil model on bench top

Figure 1.6: NACA 0015 two-dimensional airfoil model used in the experiment [5]

Blowing is often counterproductive with most control results worse than the baseline airfoil. Leading edge blowing increases the lift by generating greater circulation, but at the cost of significantly increasing leading edge pressure, therefore, the flow is more detached and the profile drag increases. Downstream blowing can improve the lift and drag characteristics, but smaller amplitudes are better than larger ones. From an amplitude perspective, larger amplitude blowing results in a larger impact on the flowfield around airfoil. For perpendicular suction, it is reported that optimum control amplitudes range between 0.01 and 0.2; values exceeding 0.2 no longer manipulate the separation bubble for perpendicular suction. For downstream tangential blowing, smaller blowing amplitudes appear to be more effective.

The use of active flow control approach can be further improved and fast response, closed-loop control systems can be used to control unsteady flows via active flow control devices [14]. According to Seifert et al. [19], progress in system integration, miniaturization, actuators, sensors and computation techniques enables the integration of the fast responding unsteady flow control techniques into a closed loop system. It is also emphasized that a lot of experiments are required to use fast response control systems in real-world problems. These experiments are time consuming and in some cases they do not produce repeatable results. There are many efforts to model and solve the problem of these unsteady flows using CFD however according to them; these efforts are still remote from what the real-world engineering requires. Therefore much more effort should be made before applying these innovative control systems to real-world problems.

Kaya et al. [28] have employed the Response Surface Methodology (RSM) for the optimization of periodically flapping airfoil parameters to maximize the thrust generation. In this study, it is shown that optimization using the RSM is much more efficient than the optimization with the steepest ascent method. The RSM allows obtaining optimum parameters with similar accuracy by performing less number of computational evaluations.

1.4 Objective of the Thesis

The experimental and numerical studies performed on synthetic jet applications over airfoil profiles have proven that the aerodynamic performance of an airfoil can be increased significantly. The parametric study performed earlier [29] shows that the synthetic jet parameters

such as the jet velocity, the jet frequency and the jet angle must be optimized to obtain the maximum aerodynamic performance. The effectiveness of a synthetic jet depends on the jet velocity, jet location, jet slot size, jet angle and jet frequency. In this study, flow control with a synthetic jet applied over a NACA 0015 airfoil is studied. The unsteady flow over the NACA 0015 airfoil is solved using a Navier-Stokes solver. Computations are performed in parallel in a computer cluster. The jet velocity, the jet frequency, the jet angle and the jet location are taken as the optimization parameters. The jet slot size used as a dependent variable and all parameters are varied in a physically acceptable range such that the power coefficient of the synthetic jet is kept constant in each case. The RSM is used in the calculation of the optimum synthetic jet parameters. The optimization is carried out at three angles of attack values ($\alpha = 10^{\circ}$, $\alpha = 14^{\circ}$, $\alpha = 18^{\circ}$) starting from pre-stall angle of attack and going up to post-stall angle of attack. The objective of the optimization is to determine synthetic jet parameters that maximize the lift to drag ratio.

CHAPTER 2

FLOW SOLUTION METHOD

2.1 Introduction

In this chapter, the Navier-Stokes flow solver used in the study is introduced. The turbulence model used in the numerical study is explained. The parallel processing and some important issues concerning the parallelization are presented. The computational grids and their generation are explained. Finally, the boundary conditions employed are described.

2.2 Navier-Stokes Solver

The numerical simulation of the flow control is performed by a 2D Navier-Stokes flow solver. The Reynolds-Averaged finite difference form of unsteady Navier-Stokes equations is solved using a C-type grid over an airfoil. Flow variables are non-dimensionalized with the freestream values of density (ρ_∞), speed of sound (a_∞), viscosity (μ_∞) and airfoil chord length (c). The non-dimensional flow variables are given as follows:

$$\rho = \frac{\rho^*}{\rho_\infty}, \quad \mathbf{u} = \frac{\mathbf{u}^*}{a_\infty}, \quad e = \frac{e^*}{\rho_\infty a_\infty^2} \tag{2.1}$$

$$t = \frac{t^* a_\infty}{c}, \quad \mu = \frac{\mu^*}{\mu_\infty} \tag{2.2}$$

where ρ^* is the density, $\mathbf{u}^*$ is the velocity, e^* is the total energy per unit volume, t^* is the time and μ^* is the viscosity.

The governing equation for 2D Navier-Stokes Equations in the curvilinear coordinates (ξ, ζ) are given as follows [30];

$$\delta_t \hat{Q} + \delta_\xi \hat{F} + \delta_\zeta \hat{G} = \frac{1}{Re}\delta_\zeta \hat{S} \tag{2.3}$$

where the Reynolds Number is defined by:

$$Re_\infty = \frac{\rho_\infty u_\infty c}{\mu_\infty} \tag{2.4}$$

where μ_∞ is the freestream dynamic viscosity.

The pressure is calculated as follows using the equation of state for an ideal gas;

$$p = (\gamma - 1)\left[e - \rho(u^2 + \omega^2)/2\right] \tag{2.5}$$

with u, ω being the components of the velocity vector, **u**.

2.2.1 Turbulence Modeling

In the flow solutions, the flow is assumed to be fully turbulent and no transition model is implemented. One equation Spalart-Allmaras turbulence model [31] is used. The Spalart-Allmaras turbulence model solves a transport equation for $\overline{\nu}$ which is related to the eddy viscosity. The transport equation for ν is given by;

$$\frac{d\overline{\nu}}{dt} = \frac{1}{\sigma}\left[\nabla \cdot ((\nu + \overline{\nu})\nabla\overline{\nu}) + c_{b2}(\nabla\overline{\nu})^2\right] + c_{b1}\overline{S}\overline{\nu}(1 - + f_{t2}) -$$

$$\left[c_{w1} f_w - \frac{c_{b1}}{\kappa^2} f_{t2}\left[\frac{\overline{\nu}}{d}\right]^2 + f_{t1}(\triangle q)^2\right] \tag{2.6}$$

where the eddy viscosity is given by;

$\nu_t = \overline{\nu} f_{v1}$ and $f_{v1} = \dfrac{\chi^3}{\chi^3 + c_{v1}^3}$ with $\chi = \dfrac{\overline{\nu}}{\nu}$.

The functions and constants appearing in the transport equation are also given as follows;

$$\overline{S} = S + \frac{\overline{\nu}}{\kappa^2 d^2} f_{v2} \qquad S = \left| \frac{\delta v}{\delta x} - \frac{\delta u}{\delta y} \right| \qquad f_{v2} = 1 - \frac{\chi}{1 + \chi f_{v1}} \tag{2.7}$$

$$f_w(r) = g\left(\frac{1 + c_{w3}^6}{g^6 + c_{w3}^6} \right)^{\frac{1}{6}} \qquad g = r + c_{w2}\left(r^6 - r\right) \qquad r = \frac{\overline{\nu}}{\overline{S}\kappa^2 d^2} \tag{2.8}$$

$$f_{t2} = c_{t3} \exp\left(-c_{t4}\chi\right) \qquad f_{t1} = c_{t1} g_t \exp\left(-c_{t2} \left(\frac{w_t}{\triangle q} \right)^2 \left(d^2 + g_t^2 d_t^2 \right) \right) \qquad \sigma = \frac{2}{3} \tag{2.9}$$

$$c_{b1=}0.1355 \qquad c_{b1=}0.622 \qquad c_{w1=}\frac{c_{b1}}{\kappa^2} + \left(1 + c_{b2}\right)/\sigma \qquad c_{w2=}0.3 \qquad c_{w3=}2 \tag{2.10}$$

$$c_{t1=}1 \qquad c_{t2=}2 \qquad c_{t3=}1.1 \qquad c_{t4=}2 \qquad \kappa = 0.41 \qquad c_{v1=}7.1 \tag{2.11}$$

2.3 Grid Generation

In this study, a structured, C-type grid is employed in the solution of flows around airfoil. High velocity and pressure gradients are encountered at the synthetic jet location and at the leading and trailing edges therefore the computational grid is refined around these locations.

The grid generation is completed in a few steps. The airfoil profile for the NACA 0015 is created using a NACA airfoil generator. The grid distribution around airfoil is modified by using an in-house code which allows rearranging the grid distribution in circumferential direction. The grid resolution is increased around the jet location, at the leading and trailing edges. Then using a FORTRAN routine, a wake is created which extends 10 chords away from the airfoil trailing edge. The spacing between the first 2 points of the wake is equal to the spacing between the last 2 points of the airfoil trailing edge. The growth ratio is taken to be 1.15. The volume grid is generated using a code called as HYPERGRID which takes the grid distribution in the circumferential direction as an input and generates the volume grid with a specified stretching ratio. The stretching ratio is specified implicitly by specifying the total thickness, total number of points and the thickness of the first and the last cells. The

input for the HYPERGRID is prepared such that a stretching ratio of 1.15 is achieved. This finalizes the grid generation process and Figure 2.1 shows a typical grid around NACA 0015 airfoil. Figure 2.1(b)illustrates the refined grid around the jet location (12% of chord).

2.4 Parallel Flow Solutions

Parallel processing is a technology which enables solving large scale and time consuming problems by dividing it into many small tasks [32]. Ideally, parallel processing makes a program run faster since multiple workstations are combined into a parallel computer. Run time of a computational evaluation is very important in the CFD applications since it is used instead of wind tunnel experiments. It is therefore desired to obtain maximum number of outputs in the minimum time. This becomes vital in an optimization problem since many computational evaluations are required.

In this study, Parallel Virtual Machine (PVM) message passing library routines are used in parallel computations. The idea behind the PVM is based on the concept of distributed memory. The PVM follows the master-worker paradigm. In a master-worker program model, there is a master node which divides the main work into pieces of sub-works and sends the sub-domains to the workers. Then the job of each sub-domain is assigned to a processor which is called as the worker [33]. The worker node computes the flow and exchanges the boundary info with the neighboring sub-domains. In other words, the master node acts as an organizer. It assigns jobs to the workers, gets the partial results from each worker. The PVM finally combines the results by applying the proper grid interface boundary conditions to generate the solution of the whole problem. There are some issues related to parallelization that can affect the computation time required.

2.4.1 Domain Decomposition

In the parallel solution of the problem, the domain decomposition technique is used. In the domain decomposition method, the primary aim is to have a grid consisting of sub-domains that have approximately the same number of points. Another issue that should be considered is the number of points in the direction perpendicular to the wall. At the interface of each sub-domain, the data coming from neighboring sub-domain is used. The communication

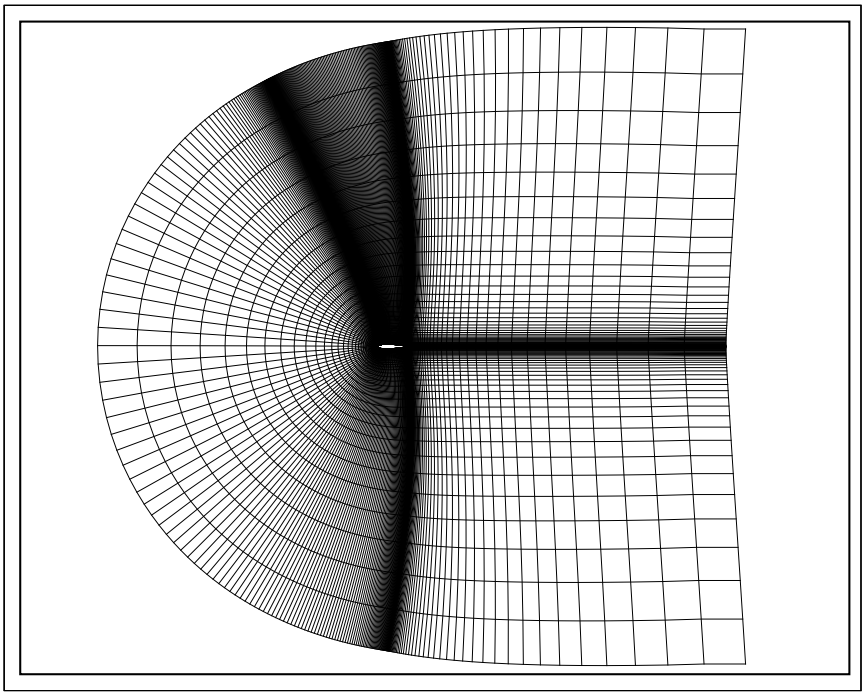

(a) Around airfoil

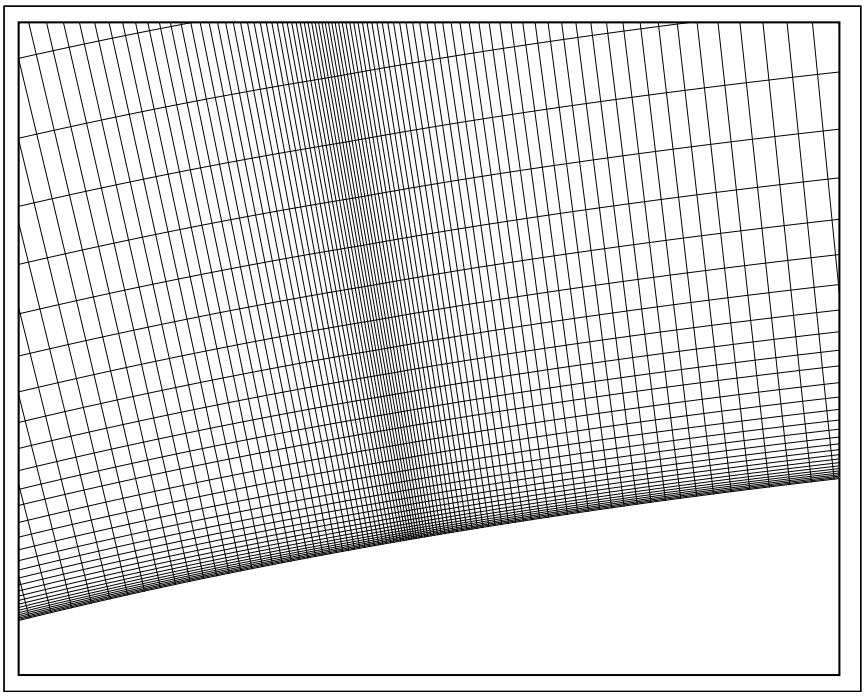

(b) Around jet location

Figure 2.1: A typical C-grid for NACA 0015 airfoil

time between the processors can be minimized by keeping the number of grid points at the interface of each block as small as possible [34]. This issue is more important for unstructured grids. A structured grid is used in this study therefore both sides of the block contains equal number of grid points and the condition of having minimum number of interface grids is automatically satisfied. While splitting the grid into a number of blocks, dividing the grid from the least critical locations is another important issue that should be taken into account. The computational domain is divided into at least 3 and at most 5 sub-domains. In order to minimize the computational error at the grid interfaces, the synthetic jet location, the leading and the trailing edges are kept in single blocks. The maximum effort is spent to equalize the size of each block however a certain amount of load imbalance may be observed in the decomposed computational domain because of the sub-domains that include highly refined grid. A typical view of domain that is decomposed into 3 blocks is shown in Figure 2.2. It is observed that the jet location, the leading and the trailing edges are kept in single blocks.

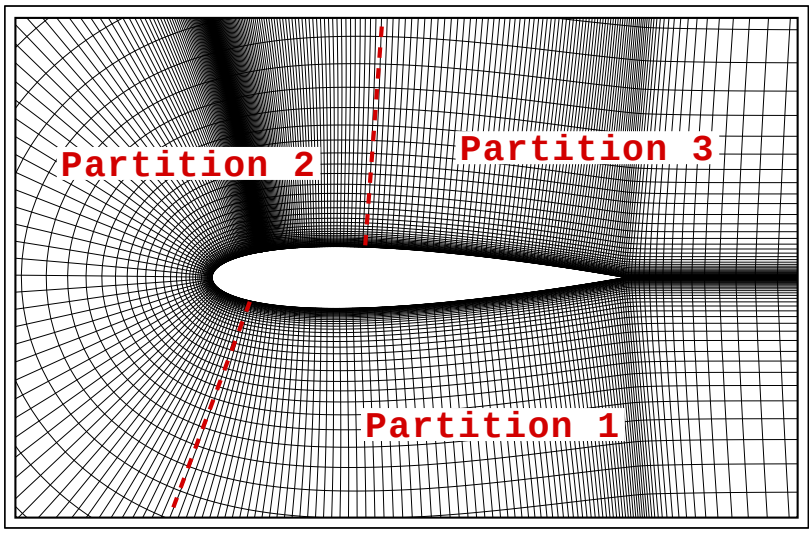

Figure 2.2: Computational domain decomposed into 3 blocks

2.4.2 Parallel Computing Environment

The parallel computing environment consists of networked PCs running a Linux operating system. There are 3 computers (atmaca 4x series) with dual Xeon processors and 16GB total memory. Each processor has 4 CPU's with 2.33 GHz speed. The data between processors is transferred by a 1 Gbps ethernet switch.

2.5 Boundary Conditions

The numerical implementation of the boundary conditions requires a particular attention. The following types of boundary conditions are used in the solution of Navier-Stokes equations:

- Wall boundary conditions
- Grid block interface boundary conditions
- Farfield boundary conditions
- Synthetic jet boundary conditions

For a viscous fluid over a solid wall, the relative velocity between the surface and the fluid at the surface is assumed to be zero which in common-terminology corresponds to the so-called no-slip boundary condition. Velocity components at the wall surface given as; u=w=0, where u is the velocity parallel to the wall and w is the velocity perpendicular to the wall [35]. Also the density and the pressure gradients are set to zero in order to define the solid wall physically.

Since the domain is split into certain number of sub-domains, the solution in the physical solution will depend on the flow in neighboring blocks. Therefore, the information between all sub-domains should be transferred correctly. The conservative flow and turbulence variables at the neighboring cells are used as the interface boundary conditions.

At the farfield boundaries, Riemann invariants which assume 1D flow at the outer boundary are employed.

The synthetic jet is implemented as a boundary condition to the flow solver. The velocity distribution of the synthetic jet is assigned to the cells defining the synthetic jet slot. The jet velocity, the jet location, the jet angle, the jet frequency and the spatial variation of the synthetic jet are the parameters used in the representation of the synthetic jet. The implementation of the synthetic jet is further explained in the Chapter 3.

CHAPTER 3

SYNTHETIC JET IMPLEMENTATION

3.1 Introduction

In this chapter, the implementation of the synthetic jet to the flow solver is described. The parameters used in the definition of the synthetic jet are described. Various synthetic jet profiles are implemented and compared against the experimental jet profile.

3.2 Synthetic Jet Implementation

Realistic implementation of the synthetic jet to the flow solver is an important issue in the simulation of the flow control. The synthetic jet is defined as a boundary condition at a specified location on the airfoil surface. The no-slip boundary condition applied on the airfoil surface is not valid at the synthetic jet location since a velocity vector is defined along the jet slot on the airfoil surface. The parameters used in the modeling of the synthetic jet are given below;

1. Non-dimensional jet velocity: $u_{jet}(s,t)$
2. Non-dimensional jet location: x_{jet}
3. Non-dimensional jet frequency: F_{jet}
4. Non-dimensional jet slot size: L_{jet}
5. Jet angle: α_{jet}

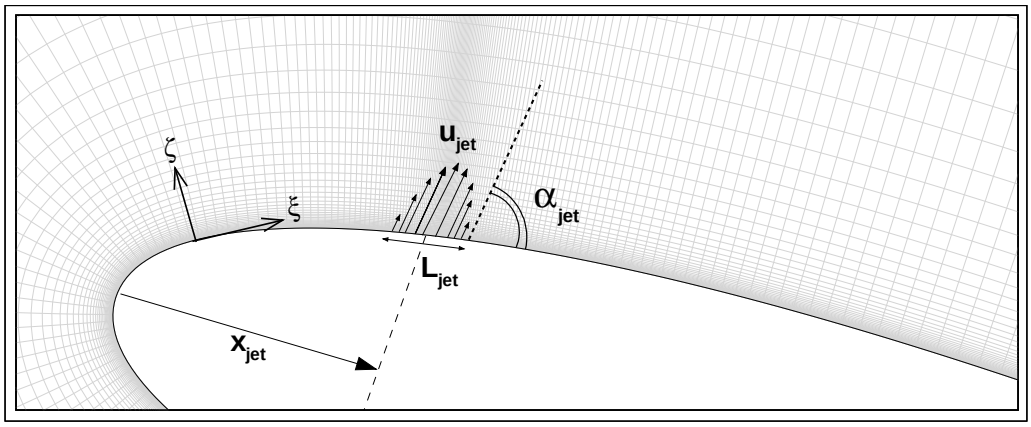

Figure 3.1: The synthetic jet representation

Figure 3.1 is a representative picture for the synthetic jet over an airfoil profile. It is observed that the grid resolution is increased at the jet location. The jet location is defined with respect to the leading edge of the airfoil. The size of the jet slot is described with L^*_{jet}. The jet angle is described as the angle between the surface of the airfoil at the slot location and the jet velocity vector. The jet velocity is defined with u^*_{jet} which corresponds to the maximum velocity for a given jet profile.

In the implementation of the synthetic jet as a boundary conditions to the flow solver, the jet parameters are non-dimensionalized except the jet angle. The freestream speed of sound (a_∞) and airfoil chord length (c) are used in the non-dimensionalization. x_{jet}, L_{jet}, u_{jet} and F_{jet} are non-dimensionalized jet parameters and defined as:

$$x_{jet} = \frac{x^*_{jet}}{c}, L_{jet} = \frac{L^*_{jet}}{c},\ u_{jet} = \frac{u^*_{jet}}{a_\infty},\ F_{jet} = \frac{F^*_{jet} c}{a_\infty} \tag{3.1}$$

The jet velocity is composed of 2 velocity components, namely mean and oscillating. An oscillatory motion is included by using a sine wave in the jet velocity expression. The expression for the jet velocity is defined as follows:

$$u_{jet} = [u_{JetMean} + u_{JetOsci} \cdot \sin(2\pi F_{jet} t)] \cdot f(s) \tag{3.2}$$

Three different actuators can be modeled with proper combinations of the mean and the oscillating jet velocities;

a) $u_{JetOsci} = 0,\ u_{JetMean} \neq 0$ for steady jet.

b) $u_{JetOsci} \neq 0,\ u_{JetMean} \neq 0$ *or* $u_{JetMean} = 0$ for oscillatory jet.

c) $u_{JetOsci} \neq 0,\ u_{JetMean} = 0$ for synthetic jet.

Spatial variation of the jet velocity (f(s)) over the slot is another parameter that can be varied. Three different spatial variations are implemented and the corresponding jet profiles are compared with the experimental jet profile obtained by Donovan et al. [13]. Following definitions are employed in expressing the variation of the synthetic jet velocity over the jet slot;

1. f(s)=1
2. f(s)=sin(πs)
3. f(s)=sin^2(πs)

The numerical jet profiles are compared with the experimental jet profile as shown in Figure 3.2. The first profile is called “top hat distribution” which is the simplest and most widely used jet profile in the literature. It is observed that the top hat distribution intersects with the experimental jet profile only at the center of the jet slot. The jet velocity at the 2 sides of the jet slot is non-zero therefore a discontinuity appears in both corners of the slot. The other jet profiles, namely the sin(πs) and the sin^2(πs) profiles are observed to be similar with the experimental profile. The f(s)=sin^2(πs) profile is the one that is most similar to the experimental jet profile. It is emphasized in the study of Donovan et al. [13] that the f(s)=sin^2(πs) profile behaves better numerically since velocity is equal to zero both on the airfoil surface and at the corner of the jet slot. The sin^2(πs) profile is therefore chosen to be used as the jet profile throughout the computational studies.

In Figure 3.3, Figure 3.4 and Figure 3.5 the schematic representation of three different actuators are shown. In all representative figures, the jet profile is plotted at different time levels (t is constant for steady jet) for $u_{JetMean}$=0, $u_{JetOsci}$=2, F_{jet}=1 and f(s)=sin^2(πs). The representative figure for steady suction and steady blowing jets given in Figure 3.3, shows that the jet

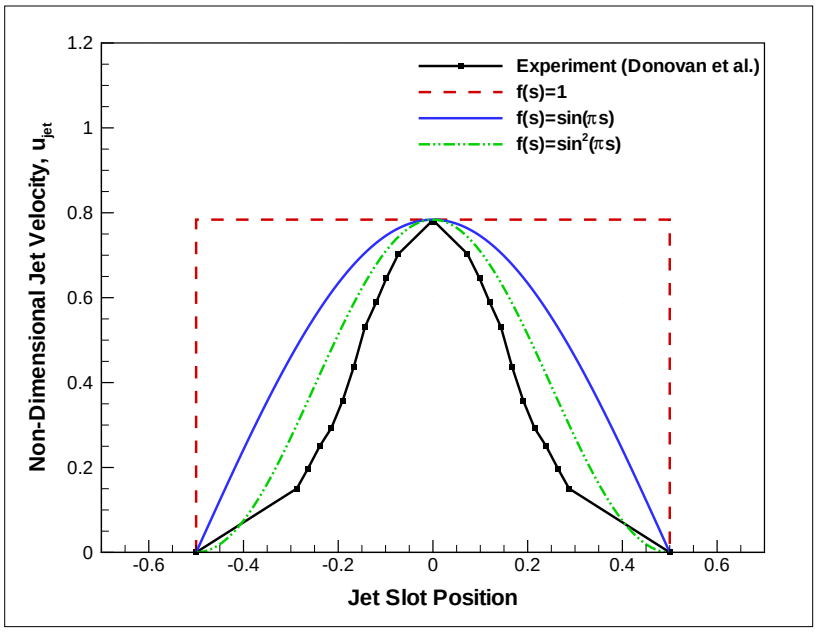

Figure 3.2: The jet profile

profile does not vary in time. The representative figure for the oscillatory jet is given in Figure 3.4. It is observed that the jet velocity oscillates around the mean velocity. Finally, Figure 3.5 represents the variation of velocity profile for a synthetic jet in time. It is observed that the magnitude of the jet velocity changes in time and the air around the actuator is sucked and blown periodically.

The jet momentum coefficient is a term that is commonly used in the definition of the synthetic jet. The expression for the jet momentum coefficient is defined as;

$$C_{\mu} = \rho_{jet} L_{let} u_{jet} \tag{3.3}$$

The power required to operate the synthetic jet is calculated by using the expression for the jet power coefficient per unit span which is defined as follows:

$$C_P = \rho_{jet} L_{jet}^2 u_{jet}^2 F_{jet} \tag{3.4}$$

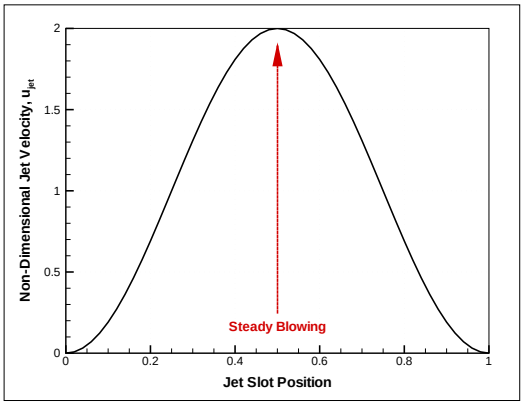

(a) Steady blowing jet

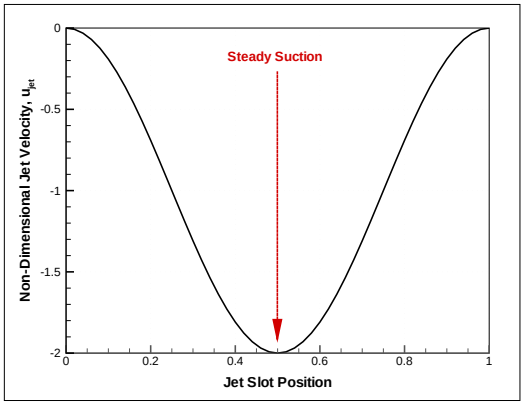

(b) Steady suction jet

Figure 3.3: Steady jets

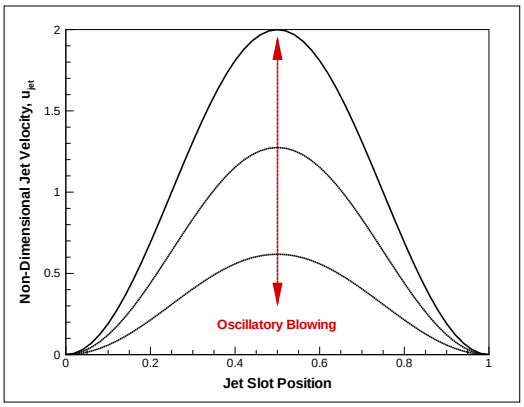

(a) Oscillatory blowing jet

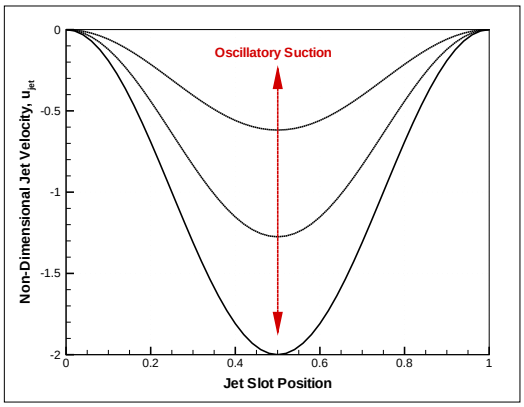

(b) Oscillatory suction jet

Figure 3.4: Oscillatory jets

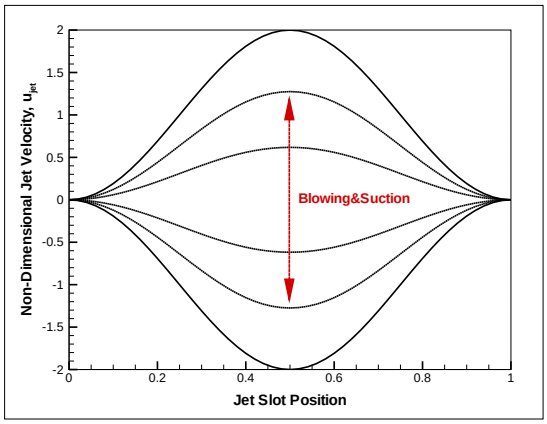

Figure 3.5: The synthetic jet

CHAPTER 4

OPTIMIZATION

4.1 Introduction

In this chapter, the optimization method employed, namely, Response Surface Methodology (RSM), is described. The optimization is based upon fitting a response surface model to the data generated using unsteady flow solver for various inputs. The response surfaces are approximated in the defined design space. The optimum design variables that maximize the value of the objective function are estimated using the response surfaces.

4.2 Response Surface Methodology

RSM is a collection of mathematical and statistical techniques that are useful in the modeling of a problem [36]. The RSM is based on the generation of response surfaces for a set of design variables. The response can be function of several variables and it can be obtained by using experimental or numerical methods. In the generation of the response surfaces, method of Least Squares is employed. Once the response surfaces are determined, the maximum or minimum values of the response and the corresponding values of optimization variables can be evaluated.

In the definition of response surface methodology, the following terminology is encountered frequently; optimization variable, response, response function. Optimization variables are process/experiment inputs whose values or settings can be controlled by the experimenter. The response is the measured quantity whose value assumed to depend on the values of optimization variables. The true value of the response, corresponding to any particular com-

bination of optimization variables in the absence of any experimental error is denoted by η. Therefore the response is function of optimization variables and mathematically it can be shown as follows:

$$\eta = f(x_1, x_2, x_3, ...x_k) \tag{4.1}$$

The function f is called the response function and it is assumed to be a continuous function of x_i. The function f that fits perfectly to the real response is usually unknown therefore it must be approximated using a polynomial or some other type of function [37].

The response surfaces are approximated by fitting a second order model to the response values. The model equation is a linear function of unknown parameters forming coefficient vector β. For example, the quadratic model with 2 optimization variables is given by:

$$y_i = \beta_0 + \beta_1 x_{1i} + \beta_2 x_{2i} + \beta_{11} x_{1i}^2 + \beta_{22} x_{2i}^2 + \beta_{12} x_{1i} x_{2i} + \varepsilon_i \tag{4.2}$$

where $i = 1, 2, ...n \geq 6$ and $\beta_0, \beta_2, \beta_{11}, ...$ are constant coefficients, y is the measured response, and $\boldsymbol{\varepsilon}$ is a random error vector used primarily to account for model's inability to approximate the real response. The matrix $\mathbf{X}$ and vector $\boldsymbol{\beta}$ can be written as:

$$\mathbf{X} = \begin{bmatrix} 1 & x_{11} & x_{21} & x_{11}^2 & x_{21}^2 & x_{11}x_{21} \\ 1 & x_{12} & x_{22} & x_{12}^2 & x_{22}^2 & x_{12}x_{22} \\ ... & ... & ... & ... & ... & ... \\ 1 & x_{1n} & x_{2n} & x_{1n}^2 & x_{2n}^2 & x_{1n}x_{2n} \end{bmatrix} \tag{4.3}$$

and

$$\boldsymbol{\beta} = \begin{bmatrix} \beta_0 \\ \beta_1 \\ \beta_2 \\ \beta_{11} \\ \beta_{22} \\ \beta_{12} \end{bmatrix} \tag{4.4}$$

In the second order model equation, the values of $\mathbf{y_i}$ and matrix $\mathbf{X}$ are known. The model is therefore fully described if the values of vector $\boldsymbol{\beta}$ can be estimated. The Method of Least Squares is used in the estimation of vector $\boldsymbol{\beta}$. Given the matrix $\mathbf{X}$, a function of the optimization variables ($\mathbf{x}$) and the vector $\mathbf{y}$ of the responses, the vector $\boldsymbol{\beta}$ is estimated by the method of Least Squares as follows:

$$\mathbf{L} = \sum_{i=1}^{n} \varepsilon_i^2 = \boldsymbol{\varepsilon}'\boldsymbol{\varepsilon} \tag{4.5}$$

where $\boldsymbol{\varepsilon}'$ is the transpose of $\boldsymbol{\varepsilon}$. The sum of squares of the errors, L can be written as:

$$\mathbf{L} = (\mathbf{y} - \mathbf{X}\beta)' (\mathbf{y} - \mathbf{X}\beta) \tag{4.6}$$

Then expanding the right hand side of that equation,

$$\mathbf{L} = \mathbf{y}'\mathbf{y} - (\mathbf{X}\boldsymbol{\beta})' \mathbf{y} - \mathbf{y}'\mathbf{X}\boldsymbol{\beta} + (\mathbf{X}\boldsymbol{\beta})' \mathbf{X}\boldsymbol{\beta} \tag{4.7}$$

$$\mathbf{L} = \mathbf{y}'\mathbf{y} - \boldsymbol{\beta}'\mathbf{X}'\mathbf{y} - \mathbf{y}'\mathbf{X}\boldsymbol{\beta} + \boldsymbol{\beta}'\mathbf{X}'\mathbf{X}\boldsymbol{\beta} \tag{4.8}$$

$$\mathbf{L} = \mathbf{y}'\mathbf{y} - 2\boldsymbol{\beta}'\mathbf{X}'\mathbf{y} + \boldsymbol{\beta}'\mathbf{X}'\mathbf{X}\boldsymbol{\beta} \tag{4.9}$$

The vector $\boldsymbol{\beta}$ can be found by minimizing the $\mathbf{L}$. The derivative of $\mathbf{L}$ with respect to vector $\boldsymbol{\beta}$ is calculated. Then partial derivative set equal to zero and solved for $\boldsymbol{\beta}$;

$$\frac{\partial \mathbf{L}}{\partial \boldsymbol{\beta}} = -2\mathbf{X}'\mathbf{y} + 2\left(\mathbf{X}'\mathbf{X}\right)\boldsymbol{\beta} \tag{4.10}$$

then

$$(\mathbf{X}'\mathbf{X})\boldsymbol{\beta} = \mathbf{X}'\mathbf{y} \tag{4.11}$$

Assuming $\mathbf{X}'\mathbf{X}$ is non-singular, we have the following least squares estimators.

$$\boldsymbol{\beta} = \left(\mathbf{X}'\mathbf{X}\right)^{-1}\mathbf{X}'\mathbf{y} \tag{4.12}$$

It is clear that $\mathbf{X}'\mathbf{X}$ is a square matrix and $\mathbf{X}'\mathbf{y}$ is a column vector [38]. Therefore the system of equations can be solved for $\boldsymbol{\beta}$ by using a matrix solver.

In this study, the response surface methodology is employed using MATLAB software for the optimization of a problem with 4 optimization variables. A quadratic response surface is then approximated for L/D based on the Least Square method. The quadratic equation is the function of the jet velocity, the jet location, the jet angle and the jet frequency:

$$\begin{aligned} L/D \;=\; & \beta_0 u_{jet}^2 + \beta_1 F_{jet}^2 + \beta_2 \alpha_{jet}^2 + \beta_3 x_{jet}^2 + \beta_4 u_{jet} F_{jet} + \beta_5 u_{jet}\alpha_{jet} + \\ & \beta_6 u_{jet} x_{jet} + \beta_7 F_{jet}\alpha_{jet} + \beta_8 F_{jet} x_{jet} + \beta_9 \alpha_{jet} x_{jet} + \beta_{10} u_{jet} + \\ & + \beta_{11} F_{jet} + \beta_{12}\alpha_{jet} + \beta_{13} x_{jet} + \beta_{14} \end{aligned} \tag{4.13}$$

where $\beta_0, \beta_1, ..., \beta_{14}$ are constant coefficients, L/D is the measured response.

Once the model is created, it is required to check the goodness of the model [39]. The accuracy of the RSM is validated by calculating RSM residuals which are the difference between the predicted and calculated responses. The RSM residuals are plotted against the predicted value of the response as shown in Figure 4.1(a). The error in the approximated quadratic model can be evaluated by analyzing the RSM residuals and the predicted-calculated plot. The predicted-calculated plot is illustrated in Figure 4.1(b). A perfect fit line is observed which represents the ideal design where the responses of the RSM model and the computed responses are equal. There are two 95% confidence lines where the area between them defines the region in which the errors in the predicted values are less than 5% of the mid-response value. The RSM residuals and predicted-calculated plots are generated in each optimization step. Both of the plots are analyzed to determine the accuracy of the RSM.

The optimization procedure followed throughout this study is illustrated in Figure 4.2. The optimization process starts with the definition of the problem. The variables that have the primary effect on the response are determined and proper ones are chosen as the design variables. Then the design space is constructed using a Design of Experiments (DoE) approach.

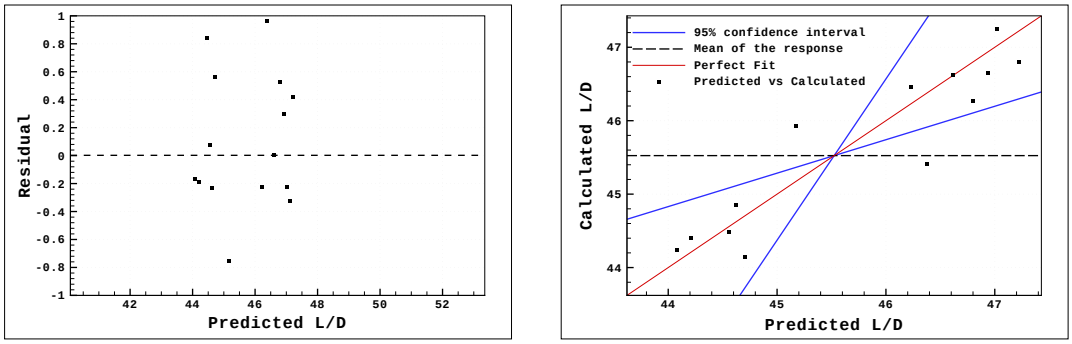

(a) A sample of RSM residuals

(b) A sample of Calculated vs. Predicted plot

Figure 4.1: RSM validation plots

Database is generated using experimental or numerical methods. In this study, the database required for RSM is generated by performing a series of CFD computations. RSM is employed for the generated database and the response surfaces are approximated. The optimum values of the design variables that maximize the response are evaluated on approximated response surfaces. Real value of the response is calculated for the optimum values of the optimization variables using experimental and numerical techniques. The error between predicted and calculated responses is calculated. The optimization process is terminated if the relative error is less than 1%. If the convergence criterion is not satisfied, a new RSM optimization is performed around the optimum point. The optimization process is carried out until the error is less than 1%.

4.3 Design of Experiments for a quadratic response surface

An experimental design for fitting a second-order model must have at least three levels of each factor. There are many Design of Experiment techniques for fitting a second order model, so it is important to choose the appropriate design. Design of experiments concerns distribution of the points in the design space [36]. The point distributions for Full-Factorial (FF) and Box-Behnken (BB) designs are shown in Figure 4.3.

In the full factorial design shown in Figure 4.3(a), the design space is covered completely. Requirement to high number of computations and being limited to low order models are the disadvantages of the full factorial design.

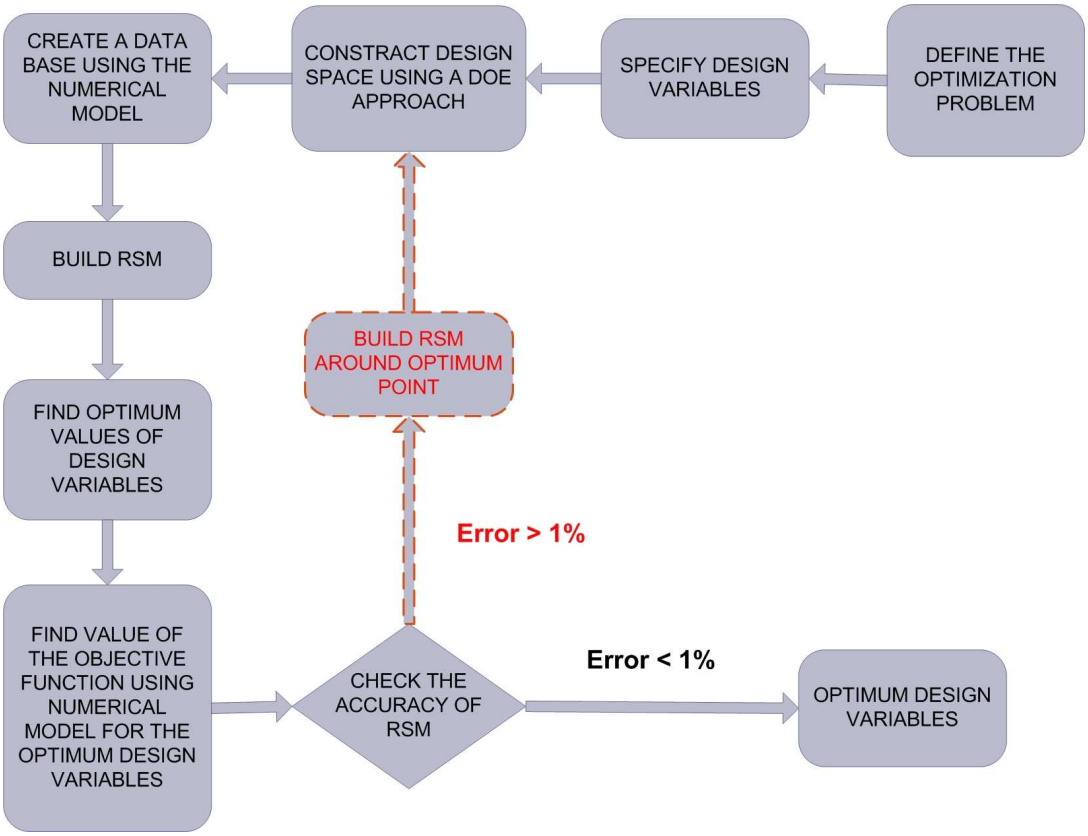

Figure 4.2: Optimization strategy

(a) Full factorial design

(b) Box-Behnken design

Figure 4.3: Designs for 3 parameters

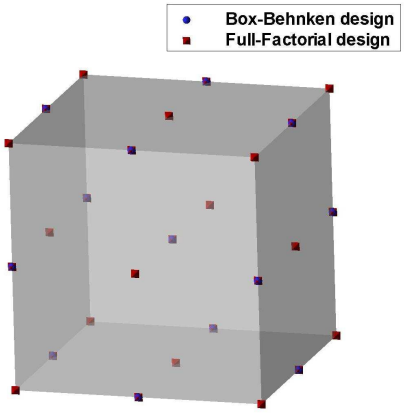

Figure 4.4: Box-Behnken and Full-Factorial designs

In the Box-Behnken design shown in Figure 4.3(b), the design points are at the midpoint of the edge and at the center. The convergence of the predicted function to real function is faster. However poor coverage of the corners of the design space is a disadvantage for the calculation of the surfaces with a badly estimated design space. The ratio of number of experiments to the number of coefficients should be in the range of 1.5 to 2.6.

The design points for the Full-Factorial and the Box-Behnken designs are shown in the same cube in Figure 4.4. The corners and face centers of the cube are not included in the Box-Behnken design.

The number of computational evaluations required for N variables are shown in Table 4.1. It is observed that the Full-Factorial design requires significantly more computational evaluations as the number of variables increases.

Table 4.1: Number of computational evaluations required for BB and FF designs

# of computational evaluations for N variables	BB	FF
3	13	27
4	25	81

CHAPTER 5

RESULTS and DISCUSSION

5.1 Introduction

Parameters defining the synthetic are optimized over a NACA 0015 airfoil to obtain the maximum lift to drag ratio for a constant jet power coefficient. Optimization is carried out using the RSM. Unsteady, turbulent flows over the NACA 0015 airfoil profile are computed using a Navier-Stokes flow solver over a C-grid. The flow is assumed to be fully turbulent and the Spalart-Allmaras turbulence model is employed. The computational domain is divided into sub-domains and the computations are performed in parallel on Linux operating system using the PVM library routines.

In unsteady calculations, the solution is initialized with the freestream conditions. The unsteady computations are carried out until a steady or a periodic behavior in aerodynamic coefficients is observed. The computed flowfields are analyzed in terms of pressure coefficient distribution, aerodynamic loads, wall shear stress and flowfields over the airfoil.

The grid sensitivity study, carried out together with the validation study, is performed by changing the circumferential and normal grid distributions with respect to a base grid. The pressure coefficient distribution, lift and drag coefficients are compared and the grid at which the computational solution becomes independent of the grid size is chosen as the optimum. The validation studies are performed for the cases with/without flow control at various angles of attack.

A parametric study is carried out to investigate the sensitivity of the solution to the synthetic jet parameters. The influence of the jet velocity, the jet location, the jet angle and the jet

frequency on the L/D is investigated. The results of the parametric study are used in the determination of the design space for the optimization study.

The synthetic jet parameters are optimized to maximize the L/D. The optimization study is performed at various angles of attack. The RSM is employed in the optimization study. The response surfaces for the L/D ratio are approximated using a second order model based on the results of the numerical model. The optimum synthetic jet parameters and the corresponding L/D values are estimated using the approximated response surfaces.

5.2 Grid Sensitivity and Validation Studies

The grid sensitivity study is performed for grid distributions in the circumferential and normal directions. The grid sensitivity study is performed by comparing the pressure distribution, lift and drag coefficients obtained with various grid sizes. The validation study is performed by comparing the results of numerical study with the experimental data. In the grid sensitivity studies, the flow over the NACA 0015 is computed at α=12° and α=22° without synthetic jet actuation. Then the computations are performed at α=16.6° for the cases with and without synthetic jet.

5.2.1 Grid sensitivity study for y^+

A grid sensitivity study is performed for the first cell size normal to the airfoil surface using 3 different y^+ values for the same surface grid distribution. The far field boundary extends up to 10 chords away from the airfoil. Table 5.1 shows the grid size, first cell size and corresponding y^+ value for each grid. The results of the computational study are compared against the experimental data of [13] for the NACA 0015 airfoil. Figure 5.1 shows the pressure coefficient distribution for M=0.15 and Re=1.2×10^6 at α=12° which is a pre-stall angle of attack for the NACA 0015 airfoil. It is observed in Figure 5.1 that the pressure coefficient at leading edge of the suction side is over-predicted and the pressure coefficient at the pressure side is in good agreement with the experiment when $y^+ \leq 0.8$. The pressure distribution over the airfoil shows that further improvement of the first cell size does not change the solution significantly after y^+=0.8. The effect of y^+ observed to be reduced at the pressure side of the airfoil since the flow is attached to the airfoil.

Table 5.1: Grid properties for the y^+ grid sensitivity study

Grid #	First cell size	y^+	Grid size
1	0.00001	0.1	378×84
2	0.0001	0.8	378×67
3	0.001	7.5	378×51

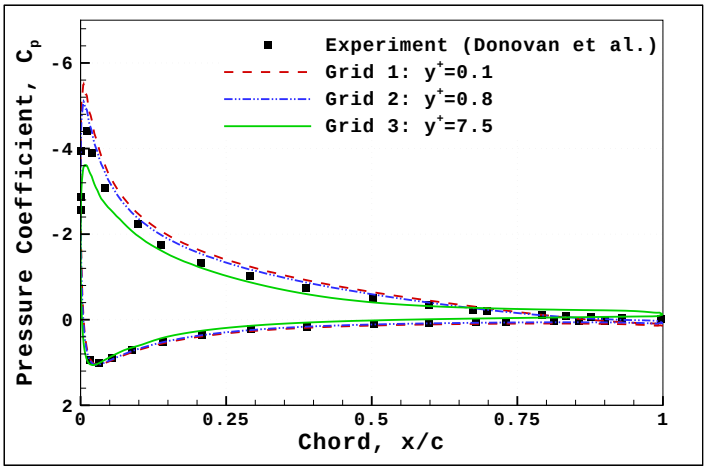

Figure 5.1: y^+ grid sensitivity, no jet (Re=1.2×10^6, M=0.15, $\alpha = 12°$)

The variation of the lift and drag coefficients are shown in Figure 5.2. The calculated lift and drag coefficients are observed to be similar for the Grid 1 and Grid 2. The optimum grid distribution in the direction normal to the airfoil surface is therefore chosen to be the grid with y^+=0.8 to be used throughout the flow computations.

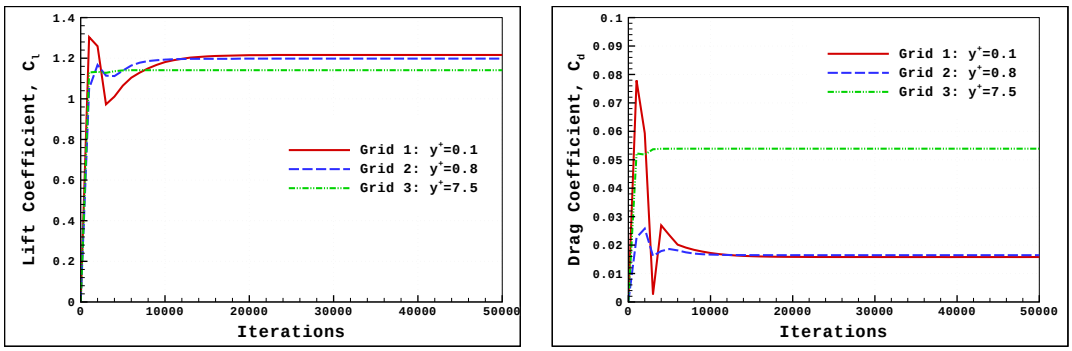

(a) Lift Coefficient (b) Drag Coefficient

Figure 5.2: Aerodynamic coefficients at $\alpha = 12°$

5.2.2 Grid sensitivity in the circumferential direction

A grid sensitivity study is performed for the grid distribution in the circumferential direction. The results of a wind tunnel test over a NACA 0015 airfoil, obtained by Gilarranz et al. [20] in a 3' x 4' wind tunnel, are used in comparisons with the present study. The experimental data is obtained at M=0.1, u_{jet}=0.231, $F_{jet} = 1.39$ and α_{jet}=16.6°. The synthetic jet is applied from the 12% of the chord and the jet slot size corresponds to 0.53% of the chord length. The properties of the grids used in the study are shown in Table 5.2. A medium grid distribution with 331 grid points in the circumferential direction is chosen as a base grid then it is coarsened/refined with a ratio of 1.5. The jet slot is defined by 12, 18 and 28 cells for the coarse, medium and fine grids, respectively. In all grids, the previously determined first cell size (corresponds to y^+=0.8) value is employed. Figure 5.3, Figure 5.5, Figure 5.7 and Figure 5.8 show the pressure coefficient distributions at various angles of attack. It is observed that the grid distribution is most effective at $\alpha = 22°$. Figure 5.5 illustrates that the results obtained with the coarse grid differs slightly more from the experimental data compared to the medium and fine grids. However, there is no difference between the results obtained with the medium and fine grids. The discrepancy between the numerical and experimental results at $\alpha = 12°$ without jet and at $\alpha = 16.6°$ with/without jet are negligible.

Table 5.2: Grid properties for the grid sensitivity in the circumferential direction

Grid	# of points around airfoil	# of points across jet slot	Grid size
Coarse	221	12	293×67
Medium	331	18	409×67
Fine	497	28	581×67

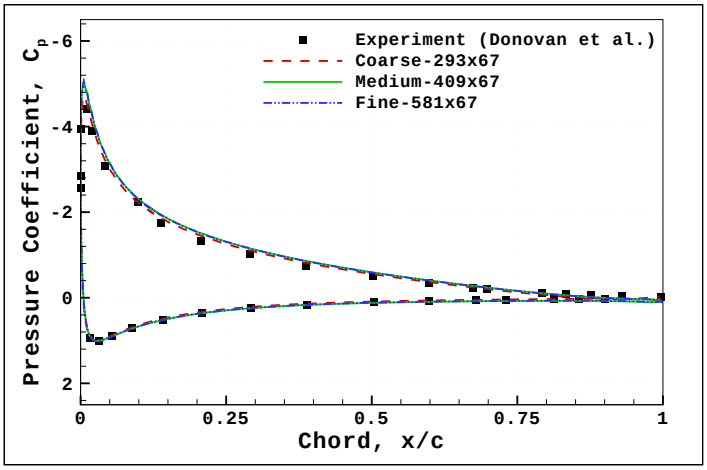

Figure 5.3: Grid sensitivity for the surface grid density, no jet (Re=1.2×10^6, M=0.15, α = 12°)

The time variations of the lift and drag coefficients are shown in Figure 5.4. The lift coefficient calculated with the medium and fine grids are similar but the coarse grid underestimates the lift coefficient. The calculated drag coefficients are observed to be same for each grid.

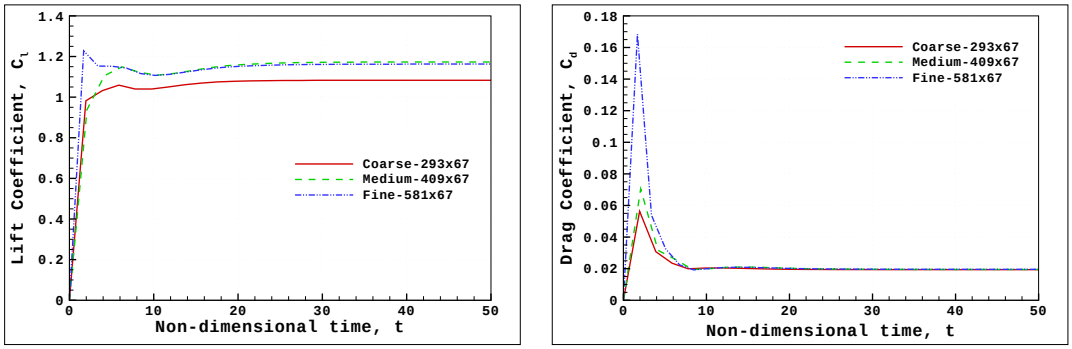

(a) Lift Coefficient (b) Drag Coefficient

Figure 5.4: Aerodynamic coefficients at $\alpha = 12°$

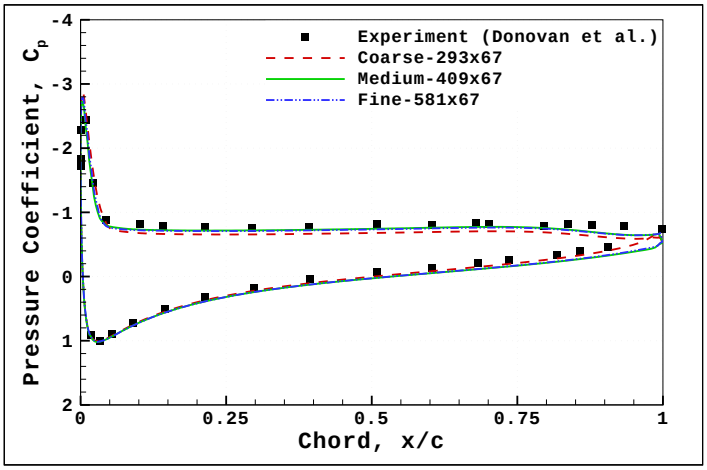

Figure 5.5: Grid sensitivity for the surface grid density, no jet (Re=1.2×10^6, M=0.15, $\alpha = 22°$)

The lift and drag coefficients presented in Figure 5.6 shows that the flowfield over NACA 0015 is unsteady at $\alpha = 22°$. The lift and drag coefficients show a periodic behavior on all grids. The average aerodynamic coefficients estimated with the medium and fine grids are observed to be same.

The pressure coefficient distributions at $\alpha = 16.6°$ are presented in Figure 5.7 and Figure 5.8 for the cases without and with the jet, respectively. The leading edge suction pressure decreases with the application of the synthetic jet in both the experimental and computational

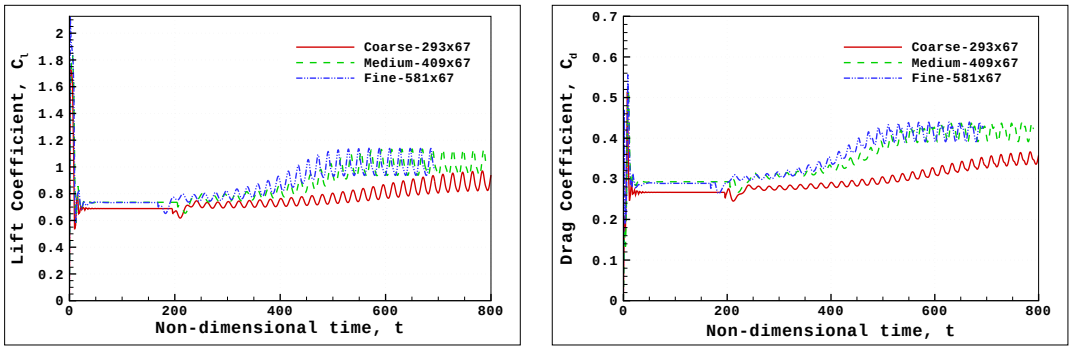

(a) Lift Coefficient (b) Drag Coefficient

Figure 5.6: Aerodynamic coefficients at $\alpha = 22°$

studies. It is thought that the synthetic jet delays the flow separation and therefore the pressure coefficient is enhanced significantly at the leading edge of the airfoil for the experimental study.

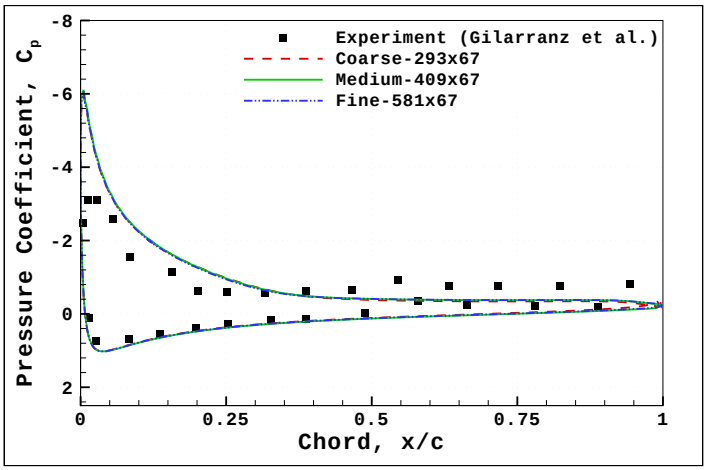

Figure 5.7: Grid sensitivity for the surface grid density, no jet (Re=822000, M=0.1, $\alpha = 16.6°$)

The time variations of lift and drag coefficients at $\alpha = 16.6°$ are shown in Figure 5.9. The lift and the drag coefficient histories with/without jet reveal that the results obtained with the medium and fine grids are similar. The flowfield over the airfoil is observed to be steady before the synthetic jet is implemented. The flowfield over the airfoil becomes unsteady with the application of the synthetic jet. Both the lift and the drag coefficients are observed to oscillate at the same frequency with the synthetic jet. The solution on the coarse grid underestimates the average lift and the drag coefficients.

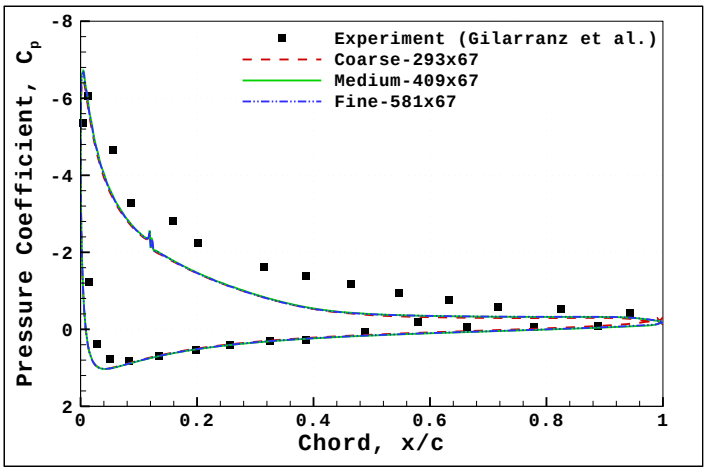

Figure 5.8: Grid sensitivity for the surface grid density, with jet (Re=822000, M=0.1, α = 16.6°, u_{jet}=0.231, F_{jet}=1.39, α_{jet} = 15°)

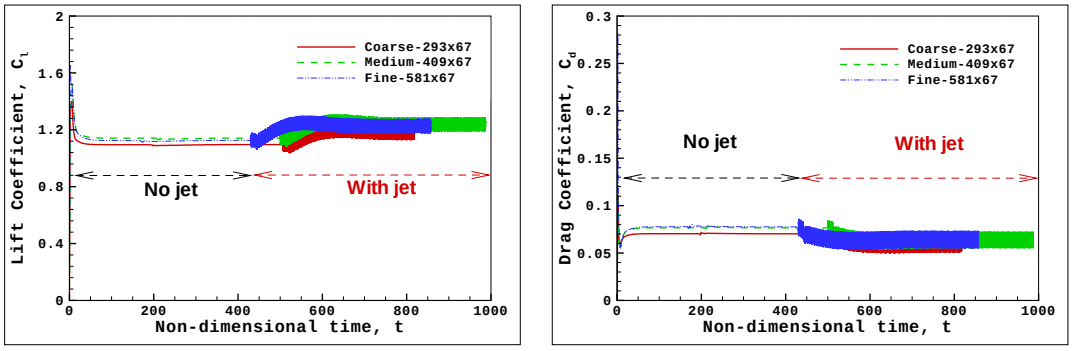

(a) Lift Coefficient

(b) Drag Coefficient

Figure 5.9: Aerodynamic coefficients at α = 16.6°

As a result of the grid sensitivity study in the circumferential direction, it is decided to use the medium size grid. The medium size grid has about 20 cells across the jet slot.

A grid convergence study is carried out in the circumferential and normal directions and the optimum values of the grid distribution in both directions are determined. Numerous computational grids are generated to be used in the parametric study for the synthetic jet location and optimization study. The grid distribution in the circumferential direction and the first cell size normal to the wall are adjusted such each grid has similar grid distributions as much as possible. The effect of grid clustering at the jet location is investigated for the cases with no flow control. It is observed that the grid clustering around jet location does not cause any numerical discrepancy in the numerical results. The same clustered grid is therefore employed in the solution of the flowfields with/without flow control.

The accuracy and range of the validity for the numerical model is determined by comparing the numerical study results with the experimental data. It is observed that the results of the present study are in good agreement with the experimental results of Donovan et al. [13] however they are not in exact agreement with the experimental data especially for the experimental results of Gilarranz et al. [20] when the synthetic jet is applied. The differences between the results of the experimental and computational studies for the NACA 0015 airfoil can be attributed to assumptions and errors that exist both on the experimental side and the numerical simulation side. On the experimental side, the installation error in the airfoil model, disturbance of the measurement device, interference between the wind tunnel wall and the airfoil body, freestream turbulence and boundary-layer trip effects can create the errors of the measurement. On the numerical simulation side, the synthetic jet modeling, the turbulence model, the grid density, the computational errors and the limitations of the two-dimensional simulation can lead to numerical inaccuracies [22].

5.2.3 Flowfield around airfoil at $\alpha = 18^\circ$

The unsteady flowfield over the NACA 0015 airfoil is computed using the optimum grid size determined in the validation study. Flowfields before and after the application of the synthetic jet are compared with the experimental data of Tuck et al. [40] at a post stall angle of attack of $\alpha = 18^\circ$ and at Re=3.08×10^4. A NACA 0015 airfoil with a chord length of 100 mm and a span of 510 mm is used. The jet slot size is reported to be 0.15% of the chord length.

The experiments were conducted in a re-circulating water tunnel with a cross sectional area of 500mm×500mm. In the experiments, the jet slot size has been minimized to obtain the maximum jet velocity. The jet slot is oriented normal to the surface of the airfoil at the leading edge, extending over the entire span of the airfoil. Particle Image Velocimetry (PIV) and Planar Laser Induced Fluorescence (PLIF) are employed in the visualization of the flow.

The averaged PLIF image and computationally obtained flowfields are shown in Figure 5.10. Both, experimental and computational flowfields demonstrate that the flow is separated at the leading edge of the airfoil when there is no synthetic jet. Formation of two vortices are observed in the streamline patterns of the present study Figure 5.10(b).

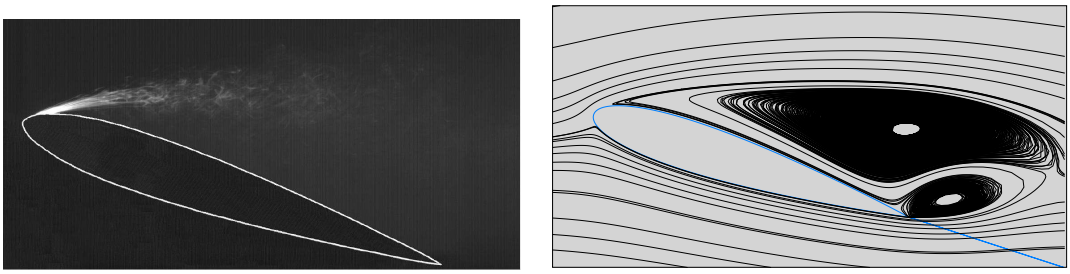

(a) Experiment (b) Computation

Figure 5.10: Averaged flowfield at $\alpha = 18°$, no jet

The flowfield through a period of the synthetic jet oscillation are shown in Figure 5.11, Figure 5.12, Figure 5.13 and Figure 5.14 for phase angles 0°, 90°, 180° and 270°, respectively. In the PLIF images shown, it is reported that the fluid ejected from the ZNMF jet orifice is observed in the external flow field at a phase angle of 90°. Similarly, the streamline patterns shown in Figure 5.12(b) obtained with the present study at a phase angle of 90° is the flowfield corresponding to the instant where the synthetic jet is starting to be blown out from the jet slot. Examination of the flowfields obtained with the experiment and the present study reveal that the vortex structures observed in the experiment differ from the ones observed in the present study. This may be attributed to the fully turbulent flow assumption without any transition modeling and also one-equation turbulence model employed.

Figure 5.15 shows the averaged flowfields when the synthetic jet is applied. The PLIF image shown in Figure 5.15(a) reveals that flow becomes attached over the upper surface of the airfoil when the synthetic jet is applied. The streamline patterns obtained with the present

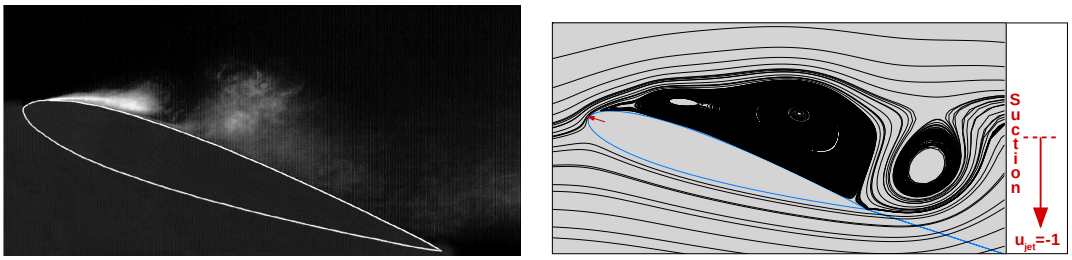

(a) Experiment (b) Computation

Figure 5.11: Flowfield at $\alpha = 18°$, phi=0°, with jet

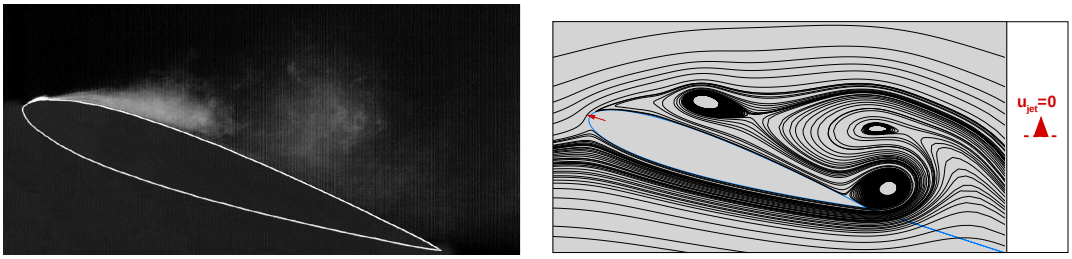

(a) Experiment (b) Computation

Figure 5.12: Flowfield at $\alpha = 18°$, phi=90°, with jet

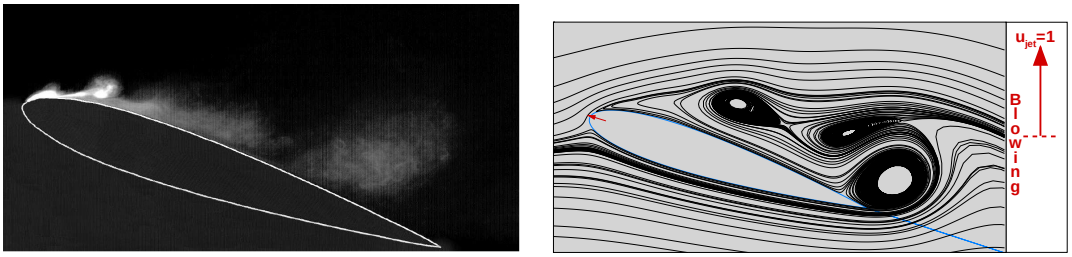

(a) Experiment (b) Computation

Figure 5.13: Flowfield at $\alpha = 18°$, phi=180°, with jet

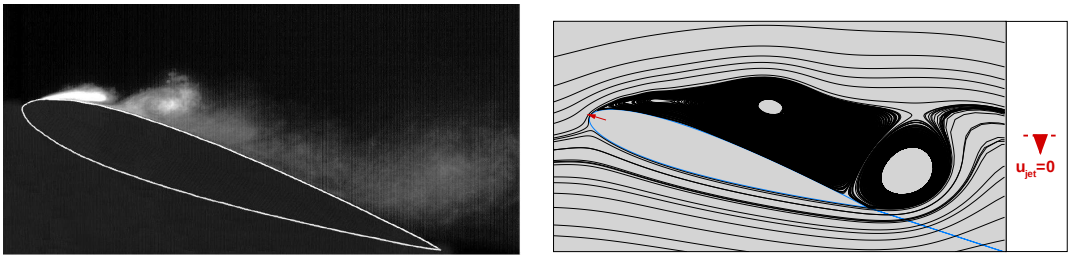

(a) Experiment (b) Computation

Figure 5.14: Flowfield at $\alpha = 18°$, phi=270°, with jet

study given in Figure 5.15(b) shows that the 2 vortices formed over the suction side of the airfoil for the case without jet(Figure 5.10(b)) reduces in size when the synthetic jet is applied. The larger vortex observed over the suction surface forms into smaller vortices similar to the case observed in the experimental study.

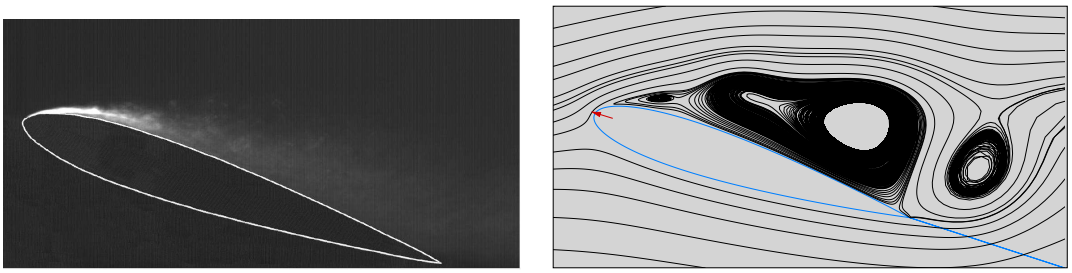

(a) Experiment (b) Computation

Figure 5.15: Averaged flowfield at $\alpha = 18°$, with jet

5.2.4 Flowfield around airfoil at $\alpha = 25°$

The results of the computational study are also compared with the experimental study of Gilarranz et al. [20] at $\alpha = 25°$. The synthetic jet is applied from 12% of the chord length with a slot size of 0.53%c. The experimental and the computational flowfields are shown in Figure 5.16 and Figure 5.17. The flow is separated at a point close to the leading edge both in the experimental and the computational results. The flow is observed to be attached in Figure 5.17(a) when the synthetic jet is applied. The flow separation at the leading edge is reduced by the presence of the synthetic jet in the computational study however the flow still separates at a point close to the leading edge as shown in Figure 5.17. The synthetic jet reduces the size of the main vortex and leads to formation of a small vortex near the leading edge.

A grid convergence study is performed for the grid distributions in circumferential and normal directions. The flowfields over the NACA 0015 airfoil are compared with the experimental flowfields at $\alpha = 18°$ and $\alpha = 25°$ where the flow over the NACA 0015 is massively separated over the suction surface in both cases. The vortex structures observed in the experimental studies are not captured exactly in the computational study which may be attributed to the solution of the flow using a RANS solver, lack of transition model and the turbulence model employed in the computational study. A more sophisticated model like LES, DNS etc. can be can be used to investigate the complex flowfields and vortex structures over the airfoil.

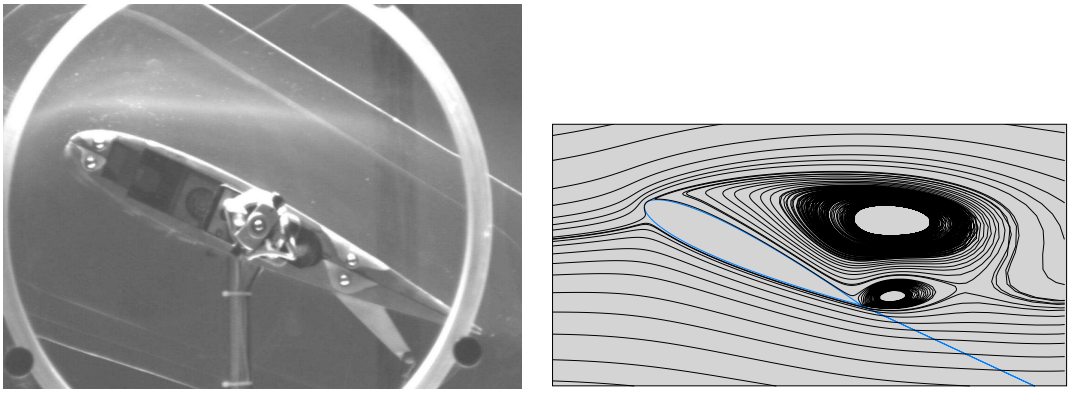

(a) Experiment (b) Computation

Figure 5.16: Flowfield at $\alpha = 25°$, no jet

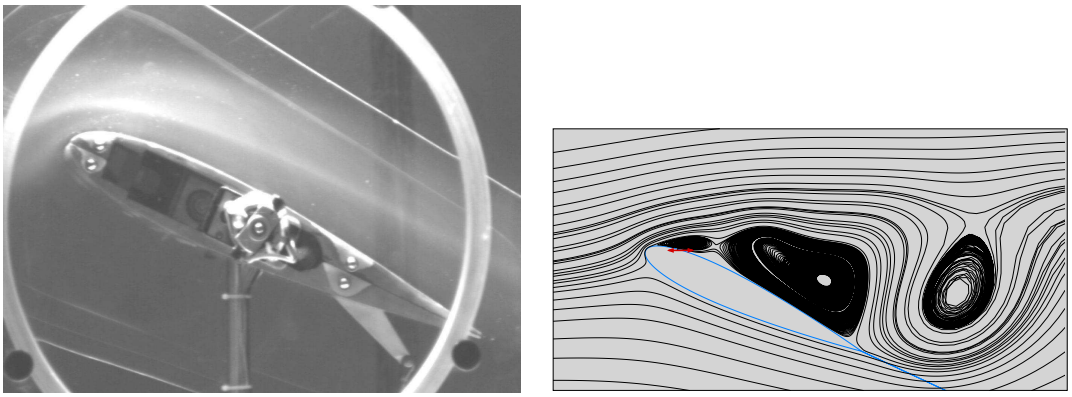

(a) Experiment (b) Computation

Figure 5.17: Flowfield at $\alpha = 25°$, with jet

5.3 Parametric study for the synthetic jet variables

A parametric study is carried out at $\alpha = 18°$ by varying the jet velocity, the jet location, the jet angle and the jet frequency to investigate the sensitivity of the jet parameters on the L/D. In the parametric studies, the NACA 0015 airfoil is used as a baseline airfoil and the flow calculations are performed at M=0.1, Re=8.96×10^5 and α_{jet}=23°. The jet slot size is chosen to be 0.53% of the chord length. The synthetic jet is applied from the 12% of the chord length in the parametric studies performed for the jet frequency, the angle and the jet velocity. In each parametric study, the value of a single parameter is changed while keeping values of the other parameters constant. The synthetic jet velocity is changed between 0.05 and 0.5. The synthetic jet location is changed between 5% and 90% of the chord. The synthetic jet angle is

changed between 10° and 98° and the non-dimensional jet frequency is changed between 0.5 and 5.

The flowfield over the NACA 0015 airfoil without application of the synthetic jet is presented in Figure 5.18 with the initial synthetic parameters of u_{jet} = 0.231, x_{jet} = 0.12, α_{jet}=23° and F_{jet} = 1.39. Two vortices are observed over the upper surface of the airfoil; one is starting from 13% of the chord and extending until the trailing edge and the other one is located at the trailing edge.

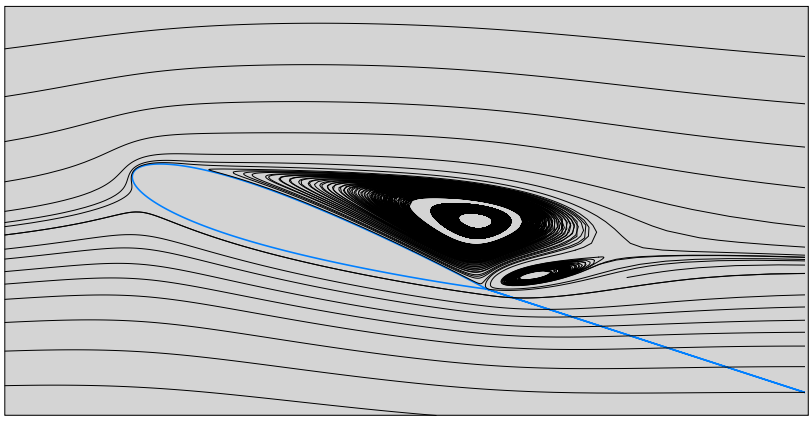

Figure 5.18: Average streamline patterns at α = 18° without synthetic jet

5.3.1 The influence of the synthetic jet velocity

The synthetic jet velocity is the first variable used in the parametric study. The synthetic jet velocity is changed between 0.05 and 0.5. Figure 5.19 shows the variation of L/D with varying synthetic jet velocity. The parametric study for the jet velocity shows that effectiveness of the synthetic jet increases as the jet velocity increases. The average streamlines shown in Figure 5.20 illustrates the flowfield over the airfoil with synthetic jet applied for u_{jet} = 0.05, u_{jet} = 0.3 and u_{jet} = 0.5. The location of the separation point is observed to move through the trailing edge of the airfoil as the jet velocity increases. It also appears that increasing the jet velocity prevents the formation of trailing edge vortex and reduces the size of the vortex formed over the airfoil upper surface. Hassan et al. [41] state that the maximum velocity that can be produced by the current synthetic jet actuators is around 0.25M which corresponds a non-dimensional jet velocity of 0.25 since M_∞=0.1. The maximum value of jet velocity is

therefore chosen to be 0.3 due to the physical limitations stated [41] and minimum value is chosen to be 0.1.

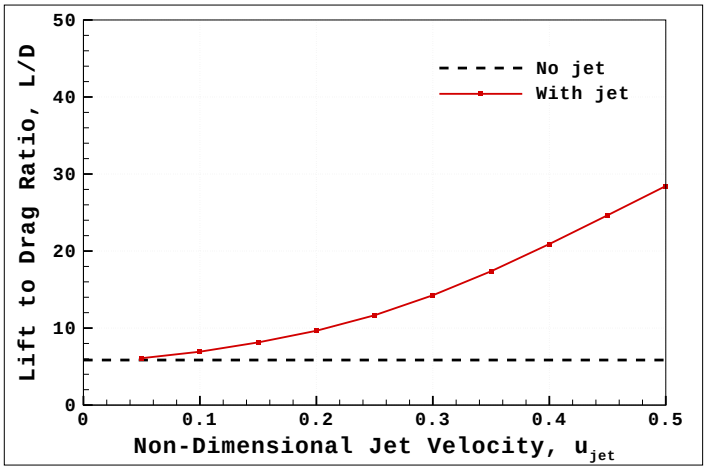

Figure 5.19: L/D variation with the velocity

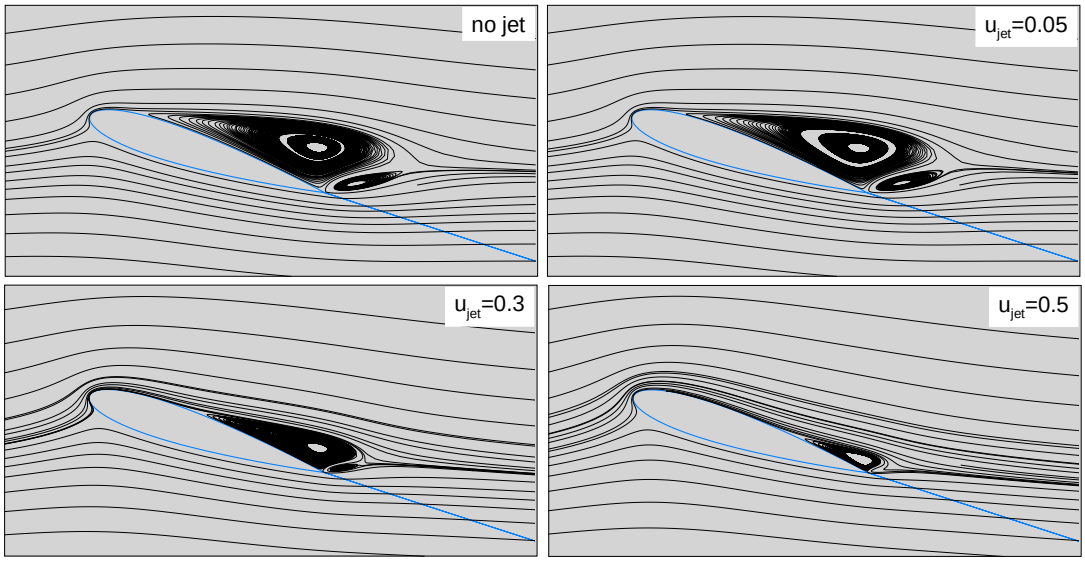

Figure 5.20: Average flowfields with various jet velocities

5.3.2 The influence of the synthetic jet location

The synthetic jet location is varied between 0% and 90% of the chord length. The variation of the L/D with the synthetic location is shown in Figure 5.21. The L/D increases by 172% compared to the case without jet when the synthetic jet is located at 30% chord location. The

synthetic jet applied from the leading edge of the airfoil caused a reduction in the L/D. It is also observed that varying the position of the synthetic jet between 50% and 90% of the chord does not cause a significant change in the L/D. The flowfields for x_{jet}=0.1, x_{jet}=0.3, x_{jet}=0.5, and x_{jet}=0.9 are illustrated in Figure 5.22. The synthetic jet located at x_{jet}=0.1 does not change the flowfield around the airfoil. Flowfield for the x_{jet}=0.3 shows that only one vortex is formed over the upper surface of the airfoil and the flowfield around airfoil is attached better compared to the no jet case. Moving the synthetic jet location to the trailing edge (x_{jet}=0.9) does not affect the location of the flow separation point.

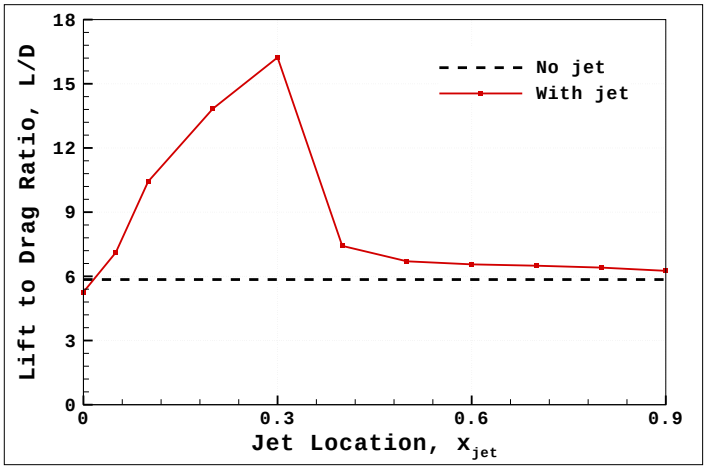

Figure 5.21: L/D variation with the location

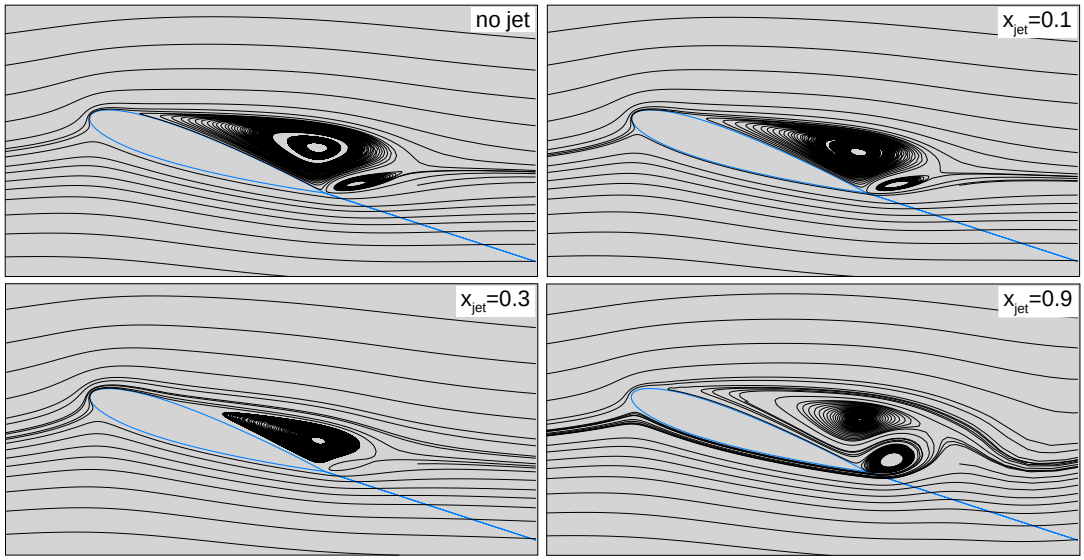

Figure 5.22: Average flowfields with various jet loactions

5.3.3 The influence of the synthetic jet angle

Then, the parametric study is performed for the synthetic jet angle where the jet angle is varied between 10° and 98°. Figure 5.23 shows the variation of L/D with varying synthetic jet angles. It is observed that, the L/D ratio is maximized when the jet angle is around 38°. The synthetic jet has a negative effect on the L/D when the jet angle is greater than 40°. The significant difference, observed in the L/D ratios of the airfoil with varying synthetic jet angle, can also be seen in the streamline patterns shown in Figure 5.24. It appears that the implementation of the synthetic jet at α_{jet}=10° and α_{jet}=83° does not change the flowfield over the airfoil and two vortices still formed over the suction side. The trailing edge vortex almost disappears and the vortex over the suction surface of the airfoil reduces in size when α_{jet}=38°.

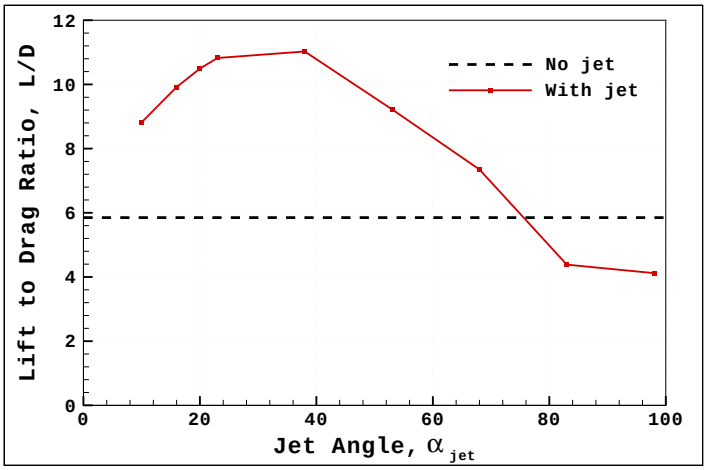

Figure 5.23: L/D variation with the jet angle

5.3.4 The influence of the synthetic jet frequency

The last synthetic jet parameter used in the parametric study is the synthetic jet frequency. The range of the jet frequency used in the parametric study is between 0.5 and 5. The variation of L/D with varying synthetic jet frequency is presented in Figure 5.25. It is observed that the synthetic jet frequency has a lower effect on the L/D but it can be said that the L/D increases as the jet frequency increases. In the experimental study performed by Gilarranz et al. [20], the frequency is reported to have a minor effect on lift coefficient and the maximum jet frequency applied is 2.39. The average streamlines for the jet frequencies of 0.5, 3 and 5

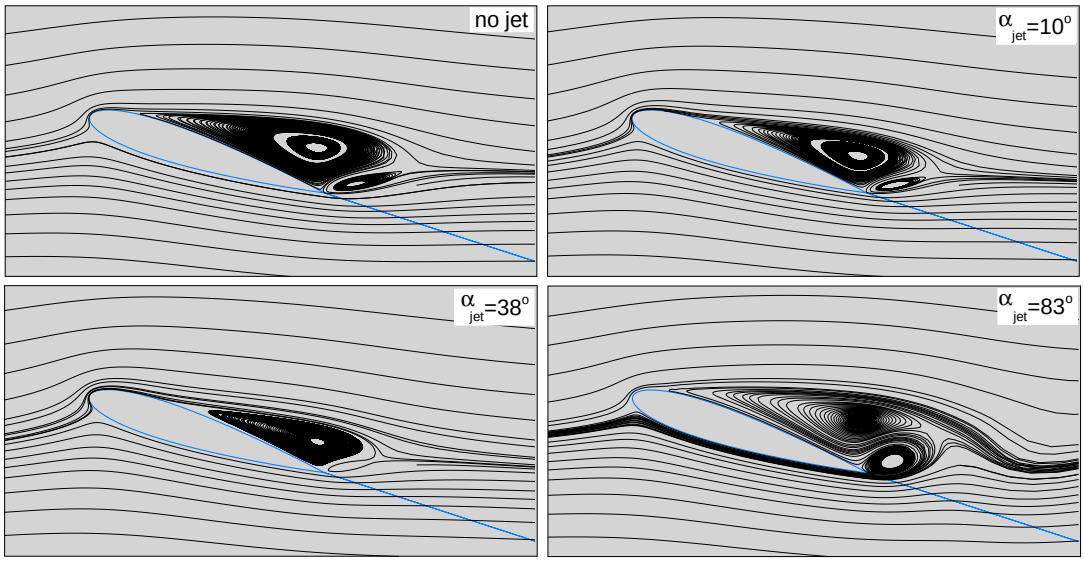

Figure 5.24: Average flowfields with various jet angles

are given in Figure 5.26. The point of separation is observed to move downstream slightly with the application of the synthetic jet however there is no significant difference between the flowfields calculated for different jet frequencies.

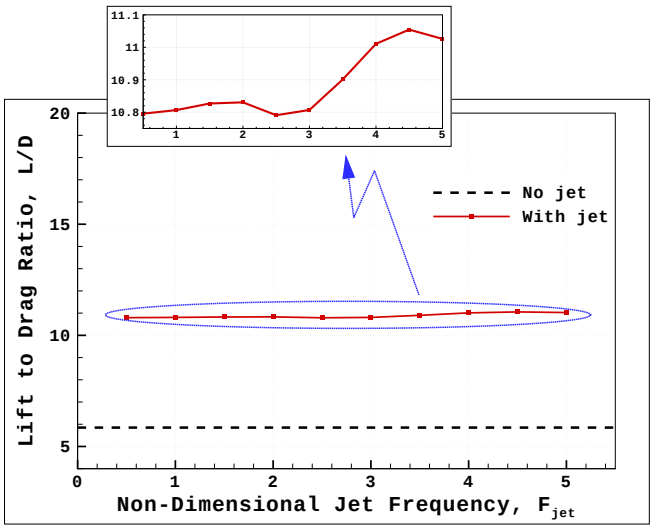

Figure 5.25: L/D variation with the jet frequency

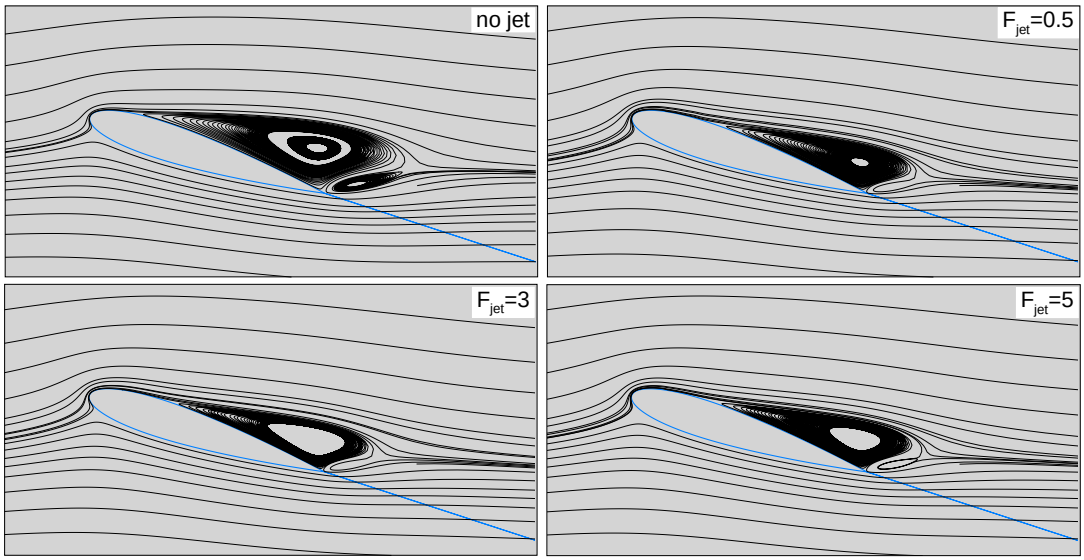

Figure 5.26: Average flowfields with various jet frequencies

5.4 Optimization of the Synthetic Jet Parameters

An optimization study is carried out to predict the optimum synthetic jet parameters to maximize the lift to drag ratio. The jet optimization study is performed for a constant value of the jet power coefficient. The jet velocity, the jet location, the jet angle and the jet frequency are the synthetic jet parameters used in the optimization study. In the optimization studies, the NACA 0015 airfoil is used as a baseline airfoil and the unsteady flow calculations are performed at M=0.1, Re=8.96×10^5. The optimization study is performed for angles of attack starting from pre-stall angle of attack, $\alpha = 10^\circ$ and going up to post-stall angle of attack, $\alpha = 18^\circ$. The cases that will be employed in the optimization study are listed in Table 5.3.

Table 5.3: Optimization cases

Case #	α (°)
1	10
2	14
3	18

The design space for the optimization study is determined by considering the results of the parametric study together with the physical limitations of the synthetic jet. Table 5.4 summarizes the design space for the synthetic jet parameters employed in the optimization study.

Table 5.4: Design space for the optimization study

Variable	Minimum value	Maximum value
Jet velocity	0.1	0.3
Jet frequency	0.8	3
Jet angle	10	50
Jet location	0.1	0.9

The optimization study is performed for a constant value of jet power coefficient (C_P=6×10^{-7}) which is the function of the density of air at the jet location, the jet velocity, the jet frequency and the jet slot size. In the computation of jet power coefficient, ρ_{jet} is assumed to be equal to the freestream density. The lift to drag ratio is optimized by varying the synthetic jet parameters in a physically allowable range while keeping the value of the jet power coefficient constant. The jet slot size is calculated for each set of optimization variables therefore it is included to the optimization study as a dependent variable. The value of jet slot size observed to be changing between 0.15% and 0.9% of the chord. The jet location is changed between 10% and 90% of the chord length for all angles of attack values. The RSM is employed in the calculation of the optimum synthetic jet parameters. The response surfaces are approximated using a 2^{nd} order model.

In the optimization study, the Box-Behnken and the Full-Factorial designs are employed in the approximation of the optimum jet parameters and corresponding L/D value at $\alpha = 18^{\circ}$ to understand the effect of DoE method. The parametric study performed for the synthetic jet velocity revealed that the L/D ratio increases with the increasing jet velocity. The optimization studies are initiated by using 4 optimization variables at all angles of attack. The optimum jet velocity is observed to be maximum value in the defined range for all angles of attack therefore 3 optimization variables are employed in the subsequent optimization steps by keeping the jet velocity constant at the maximum value. In the first step of the optimization studies, the Box-Behnken design is employed therefore 25 computational evaluations are required for 4 optimization variables. Then the Box-Behnken or the Full Factorial designs are employed for 3 optimization variables.

In each step of the optimization, the accuracy of the model is determined by calculating the error between estimated and calculated values. The optimization study is performed until the error between the estimated and the calculated values is less than 1%. If the error criterion

is not satisfied, new computational simulations are performed around the optimum point. A typical optimization step takes about 18-54 hours of wall clock time in a parallel computing environment using 3 processors.

5.4.1 Choice of Design of Experiment

The optimization study is performed using two different DoE approaches to understand the effect of DoE in the estimation of the optimum synthetic jet parameters. The Box-Behnken (BB) and the Full-Factorial (FF) designs are employed for 4 synthetic jet parameters at $\alpha = 18°$. In the Box-Behnken design, 25 computational evaluations are required for 4 design parameters. In the Full Factorial design, 81 computational evaluations are performed to approximate the response surfaces. Table 5.5 shows the values of the optimum design parameters estimated in each design. The estimated jet velocity and jet frequency are observed to be same. The optimum jet locations are estimated to be 18% and 24% of the chord for the Box-Behnken and Full-Factorial designs, respectively. The error between the estimated and calculated values is observed to be smaller for the FF design which may be attributed to the large number of computational evaluations.

Table 5.5: Box Behnken and Full Factorial Designs

Design	u_{jet}	F_{jet}	$\alpha_{jet}(°)$	x_{jet}	Estimated L/D	Calculated L/D	Error (%)
BB	0.3	3.0	40.8	0.18	19.7	11.5	71.6
FF	0.3	3.0	50	0.24	13.3	15.8	-16.2

5.4.2 Case 1: $\alpha = 10°$

The optimization study for the synthetic jet parameters is carried out first at $\alpha = 10°$ which is a pre-stall angle of attack for the NACA 0015 airfoil. The optimization study is terminated in 2 optimization steps as listed in Table 5.6. The optimization study performed for 4 optimization variables then the jet velocity is excluded and 3 optimization variables are optimized in the second optimization step. The errors between the estimated and calculated values are observed to be small in both optimization steps therefore computational evaluations performed

in the first optimization step with the maximum jet velocity are also included in the second optimization step. The optimum jet location is estimated to be 10%c which is the most forward location in the design space. The absolute error for the L/D in the second optimization step is calculated to be 0.3%.

Table 5.6: Results of the optimization steps at $\alpha = 10°$

Optimization Step	u_{jet}	F_{jet}	$\alpha_{jet}(°)$	x_{jet}	Estimated L/D	Calculated L/D	Error (%)
1	0.3	3.0	22.0	0.1	80.97	76.6	5.7
2	0.3	0.8	28.5	0.1	79.99	80.3	-0.3

The predicted-computed values and RSM residuals at $\alpha = 10°$ shown in Figure 5.27 for the second optimization step. The RSM residuals are observed to be small compared to RSM residuals at $\alpha = 14°$ and $\alpha = 18°$. The enhancement in the L/D after the application of the synthetic jet is lower therefore the response surfaces are smoother compared to the ones obtained at higher angles of attack. The better approximation of the response surfaces allows estimating the optimum variables and the responses more accurately.

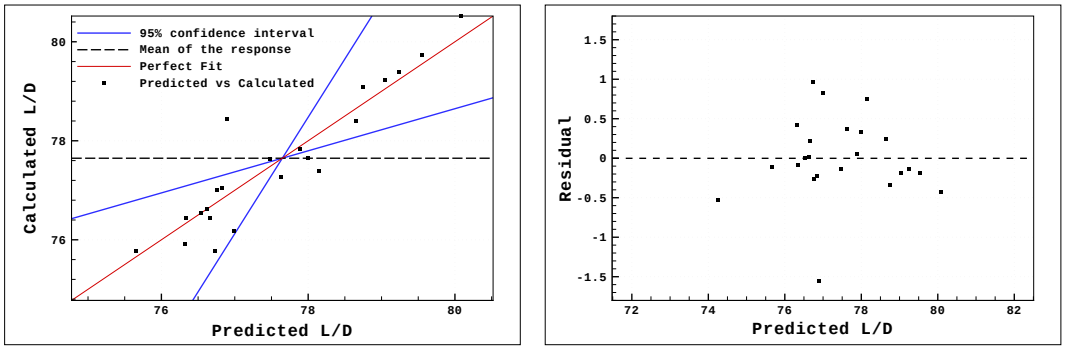

(a) Predicted-calculated values (b) RSM residuals

Figure 5.27: Optimization at 2^{nd} step at $\alpha = 10°$

The response surfaces approximated at the second optimization step are shown in Figure 5.28. It is noted that the optimum L/D is estimated at the constraint boundary for the jet velocity, the jet frequency and the jet location with α_{jet}=28.5.

The streamline patterns are shown in Figure 5.29 for the cases before and after the application the synthetic jet. The synthetic jet, applied from the 10% of the chord, is observed to be

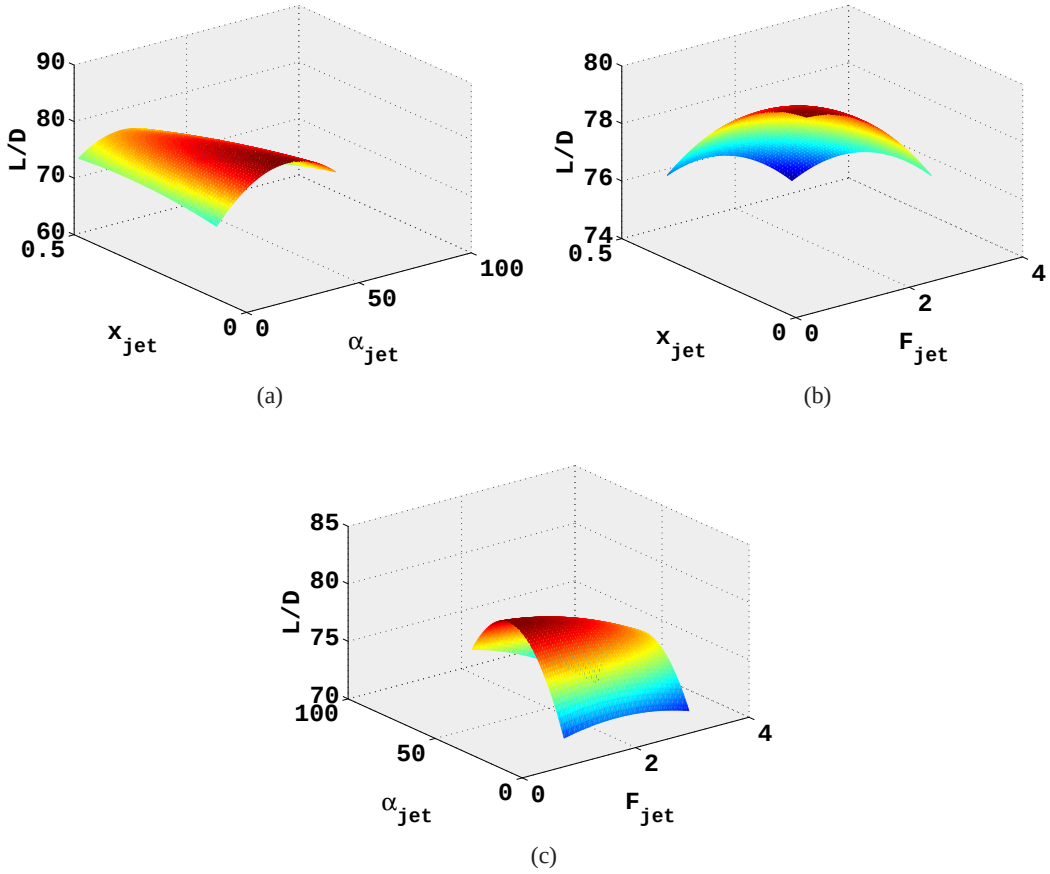

Figure 5.28: Response surfaces at 2^{nd} optimization step at $\alpha = 10°$

almost ineffective on the flowfield around airfoil.

The flow separation is delayed when the synthetic jet is applied. The location of separation point is determined by the location of zero wall-shear stress. The instantaneous skin friction coefficient variation over the upper surface of the airfoil shown in Figure 5.30 reveals that the separation point moves from 93% of the chord to the 94.3% of the chord when the synthetic jet is applied.

The variation of lift and drag coefficients in time is given in Figure 5.31. The variation in the lift and the drag coefficients is observed to be very low. The variation of the average lift and drag coefficients are given in Table 5.7. The reduction in the drag coefficient is observed to be 6.2% and the enhancement in the lift coefficient is observed to 1.5%. The increase in the L/D is 8.2%.

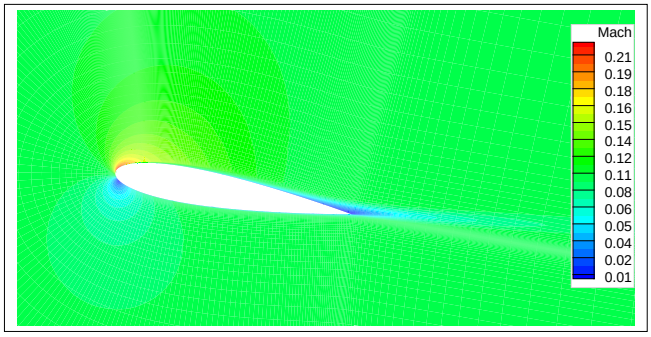

(a) No jet

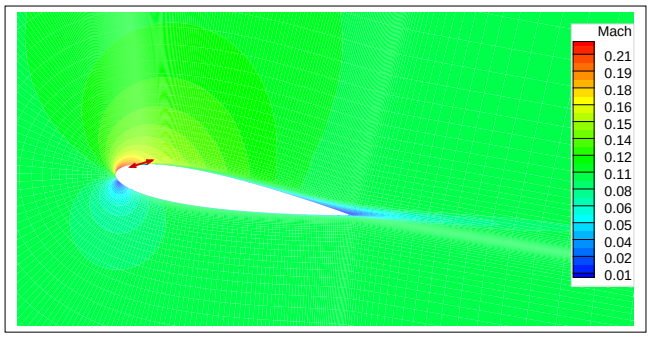

(b) With jet

Figure 5.29: Average streamline patterns at $\alpha = 10°$

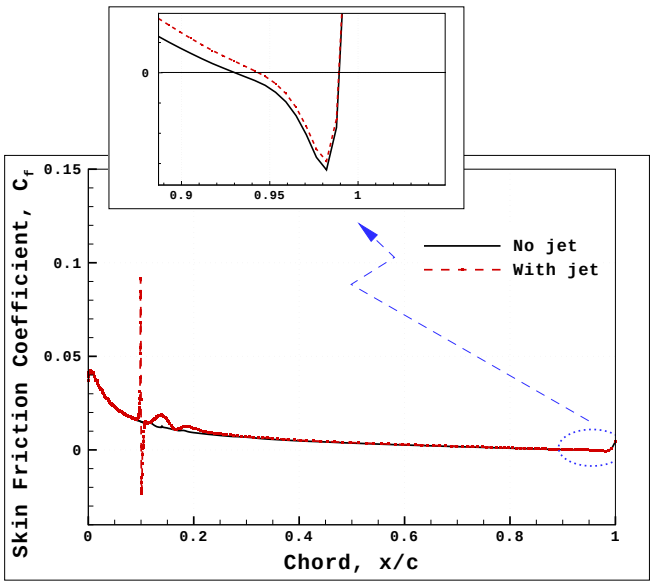

Figure 5.30: Instantaneous skin friction coefficients for the upper surface at $\alpha = 10°$

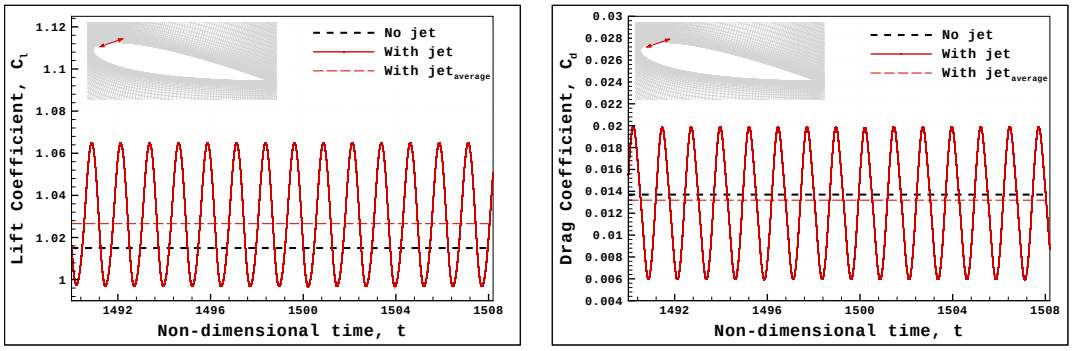

(a) Lift coefficient history

(b) Drag coefficient history

Figure 5.31: Lift and drag coefficient histories at $\alpha = 10°$

Table 5.7: Aerodynamic coefficients at $\alpha = 10°$

	C_l	C_d	L/D
No jet	1.01	0.0137	74.2
With jet	1.03	0.0128	80.3
Change(%)	1.5	-6.2	8.2

5.4.3 Case 2: $\alpha = 14°$

The optimization study is performed at 14° angle of attack. Table 5.8 shows the values of the optimum design parameters obtained through the 3 optimization steps. The Box-Behnken design is employed for 4 optimization variables in the first optimization step. Then the jet velocity is excluded and 3 optimization variables are optimized in the next 2 optimization steps. The maximum jet velocity is again estimated to be the maximum input value. The estimated value of the optimum jet location is varied between 0.4c and 0.5c through the optimization steps. The optimum value of the jet location is estimated to be 43%c in the final optimization step. The optimum jet angle is estimated to be 42.5°. The error between the estimated and the calculated values of the L/D is observed to be 0.3% at the final optimization step.

The predicted-computed values and RSM residuals at the third step of the optimization are shown in of L/D are shown in Figure 5.32. It is observed from Figure 5.32(a) most of the predicted responses are in the 95% confidence area. The RSM residuals shown in Figure 5.32(b) reveals that the maximum residual is lower than 0.4 in L/D.

Table 5.8: Results of the optimization steps at $\alpha = 14°$

Optimization Step	u_{jet}	F_{jet}	$\alpha_{jet}(°)$	x_{jet}	Estimated L/D	Calculated L/D	Error (%)
1	0.3	3.0	46.0	0.5	49.5	46.1	7.4
2	0.3	0.8	40.2	0.42	48.2	47.5	1.4
3	0.3	0.8	42.5	0.43	48.5	48.4	0.3

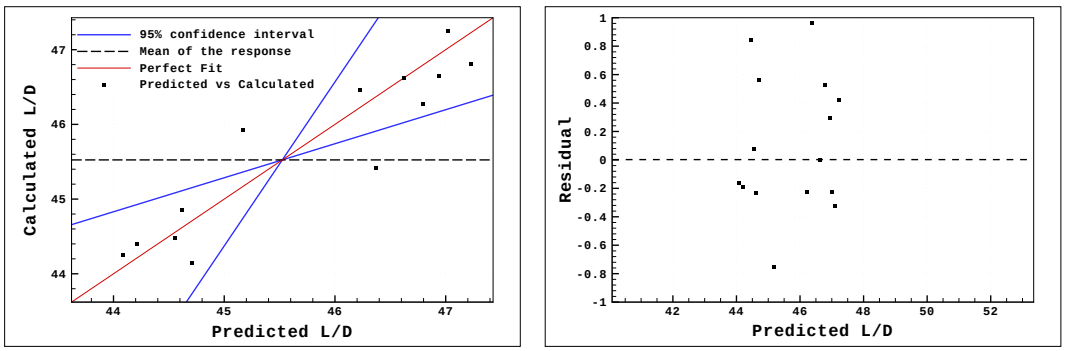

(a) Predicted-calculated values

(b) RSM residuals

Figure 5.32: Optimization at 3^{rd} step at $\alpha = 14°$

The response surfaces approximated at the third optimization step are shown in Figure 5.33. The optimum L/D is estimated when α_{jet}=42.5, x_{jet}=0.42 and F_{jet}=0.8.

Figure 5.34 shows the average streamline patterns around airfoil before and after the synthetic jet application. It is observed that the vortex formed on the suction side of the airfoil has reduced in size and moved through the trailing edge after the synthetic jet is applied with the optimum jet parameters. The small vortex observed at the trailing edge of the airfoil almost disappeared.

The instantaneous skin friction coefficient variation over the upper surface of the airfoil shown in Figure 5.35 reveals that the separation point moves from 66% of the chord to the 79% of the chord when the synthetic jet is applied.

The variation of the lift and drag coefficients are shown in Figure 5.36. The application of the synthetic jet is observed to cause an oscillation both in the drag and lift coefficients. The variation of the lift and drag coefficients are shown in Table 5.9. The reduction in the drag

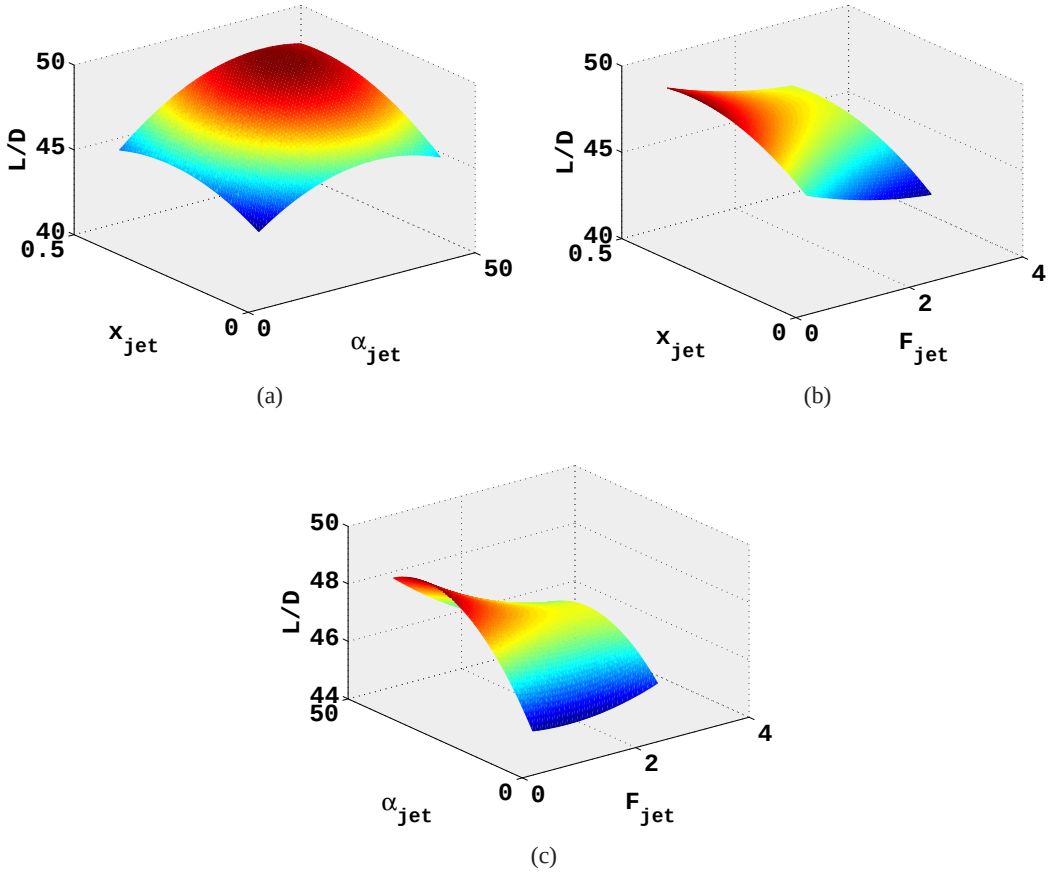

Figure 5.33: Response surfaces at 3^{rd} optimization step at $\alpha = 14°$

coefficient is observed to be 10.3% and the enhancement in the lift coefficient is observed to 5.6%. The L/D ratio is increased by 17.9%.

Table 5.9: Aerodynamic coefficients at $\alpha = 14°$

	C_l	C_d	L/D
No jet	1.27	0.031	41.1
With jet	1.34	0.028	48.5
Change(%)	5.8	-10.3	17.9

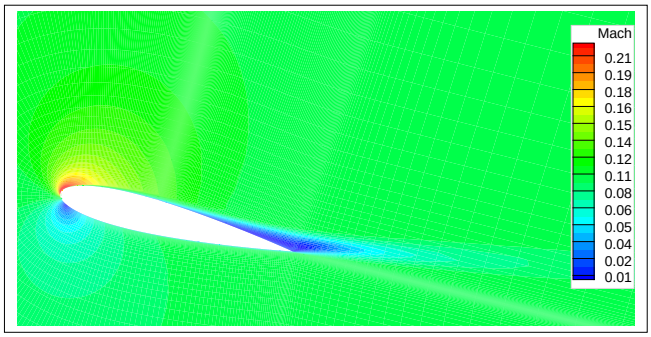

(a) No jet

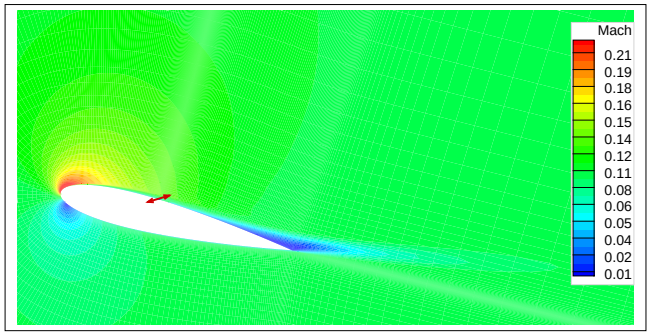

(b) With jet

Figure 5.34: Average streamline patterns at $\alpha = 14°$

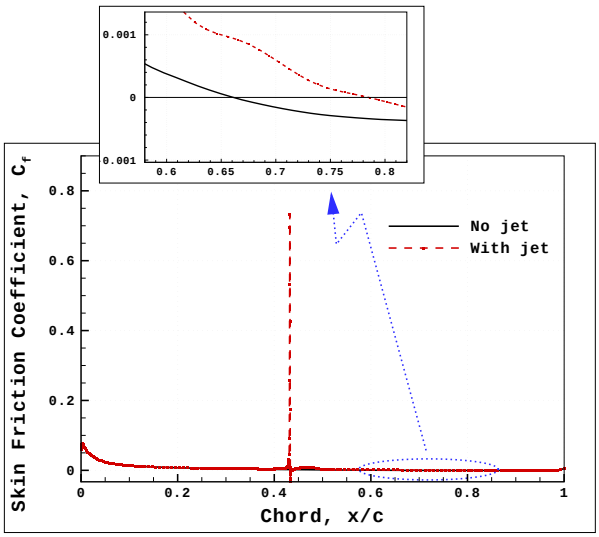

Figure 5.35: Instantaneous skin friction coefficients for the upper surface at $\alpha = 14°$

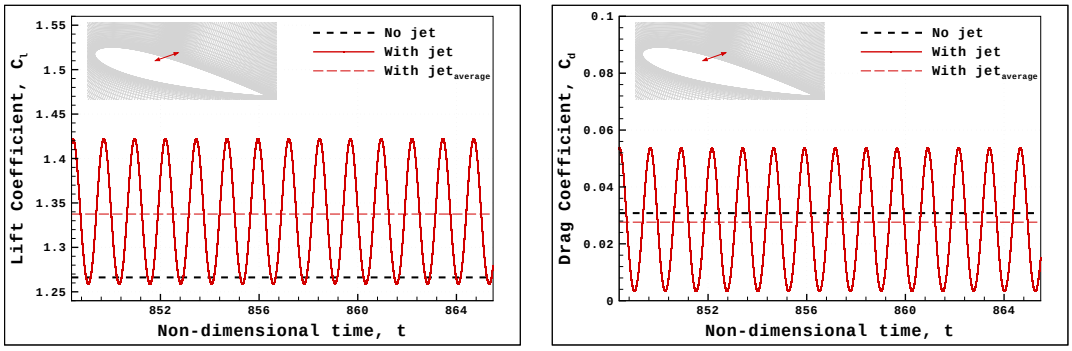

(a) Lift coefficient history

(b) Drag coefficient history

Figure 5.36: Lift and drag coefficient histories at $\alpha = 14°$

5.4.4 Case 3: $\alpha = 18°$

The optimization study is finally performed at $\alpha = 18°$ which is a post stall angle of attack for the NACA 0015 airfoil. The optimization process is terminated in 3 optimization steps. Table 5.10 shows the values of the optimum design parameters and relative errors obtained in optimization steps. In the first optimization step, the flow over NACA 0015 airfoil is computed for various optimization variables and the optimum point is calculated using Box-Behnken design. The error in the first step is observed to be 71.6%. In the second optimization step, a new RSM is employed around the optimum point estimated in first optimization step. The error is reduced to 13.9%. In the first two steps, the synthetic jet velocity is estimated to be 3 therefore the jet velocity is kept constant and Full-Factorial design is employed by varying the values the remaining 3 variables. The relative error in the third step is calculated to be 0.6% which satisfies the convergence criteria. The value of the jet angle is observed to be increasing through the optimization steps. The optimum jet location is found to be 36% of the chord length.

Table 5.10: Results of the optimization steps at $\alpha = 18°$

Optimization Step	u_{jet}	F_{jet}	$\alpha_{jet}(°)$	x_{jet}	Estimated L/D	Calculated L/D	Error (%)
1	0.3	3.0	40.8	0.18	19.7	11.5	71.6
2	0.3	0.8	41.4	0.23	17.0	14.9	13.9
3	0.3	0.8	44.7	0.36	18.3	18.2	0.6

The predicted-computed values of L/D are shown in Figure 5.37 for the second and third optimization steps. It is observed from Figure 5.37(a) that most of the estimated values fall outside of the 95% confidence interval at the second optimization step. The number of points in the 95% confidence interval increased at the third optimization step as presented in Figure 5.37(b). The number of points in the 95% confidence interval increases at the third optimization step since the approximated response surfaces becomes smoother as the design range gets smaller.

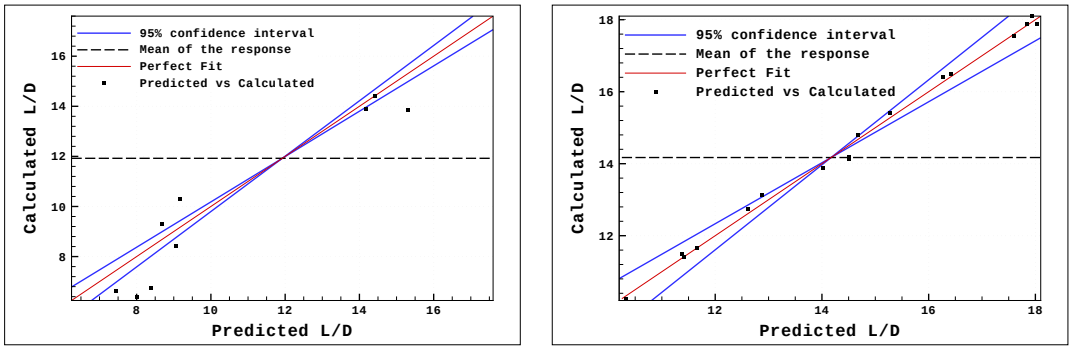

(a) The second optimization step (b) The third optimization step

Figure 5.37: Predicted-Calculated values at $\alpha = 18°$

The RSM residuals in the second and the third steps of the optimization are shown in Figure 5.38. The residual values have reduced in the third optimization since the accuracy of the approximated response surfaces increases because of the reduced range of optimization variables.

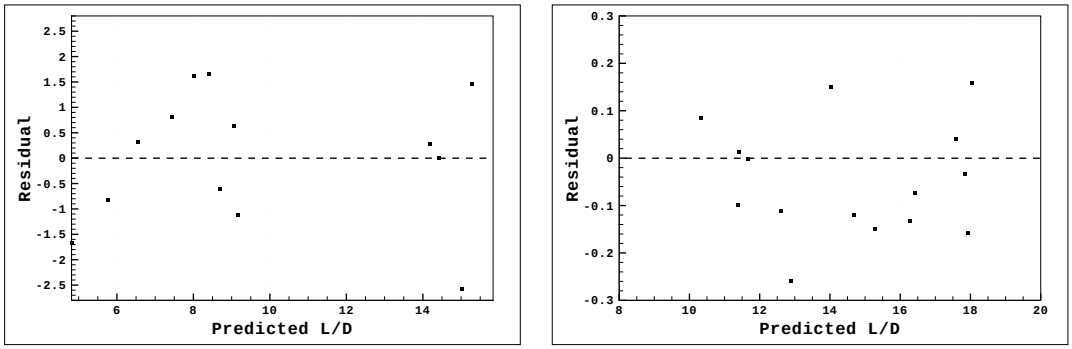

(a) The second optimization step (b) The third optimization step

Figure 5.38: RSM residuals at $\alpha = 18°$

In Figure 5.39, the response surfaces obtained in the first step of the optimization study are illustrated. It is observed that the synthetic jet velocity and the location are the effective parameters for the value of the L/D. The response surfaces are maximized as the jet velocity increases.

The RSM surfaces approximated for 3 optimization variables (when u_{jet}=0.3) at the final optimization step are shown in Figure 5.40. The RSM surfaces illustrates that the L/D is maximized when α_{jet}=44.7, x_{jet}=0.36 and F_{jet}=0.8.

Figure 5.41 shows the average streamline patterns around airfoil before and after the synthetic jet application. It is observed that the vortex formed on the suction side of the airfoil has reduced in size and moved through the trailing edge. The vortex observed at the trailing edge of the airfoil is almost disappeared.

The instantaneous flowfields along a period of the synthetic jet are given in Figure 5.42 for the optimum jet parameters. The velocity vectors at the jet location are also shown at each phase. The synthetic jet starts blowing when the ϕ=0. The jet velocity reaches to the maximum value when $\pi/2$ then suction phase starts. The streamline pattern around the airfoil observed to be almost same in a time period. It is observed that the presence of the synthetic jet moves the separation point downstream as observed from the average streamline patterns shown in Figure 5.41 previously.

The instantaneous skin friction coefficients on the upper surface of the airfoil for the cases with and without jet are shown in Figure 5.43. It is observed from the zoomed figure that the flow separates at about 13% of the chord length on the suction side of the airfoil without jet application. The separation point moves to the 33% of the chord length when the synthetic jet is applied with the optimum jet parameters.

The variation of lift and drag coefficients are shown in Figure 5.44. It is observed that both the lift and the drag coefficients oscillate at a constant amplitude and frequency when synthetic jet is applied. The frequency of oscillations is equal to the frequency of the synthetic jet. Table 5.11 shows that the application of the synthetic jet has increased the average lift coefficient by 52.6% and reduced the average drag coefficient by 51% which corresponds to 211% increase in the L/D when compared with no jet case.

The optimum synthetic jet parameters are estimated using the RSM at 3 different angles of

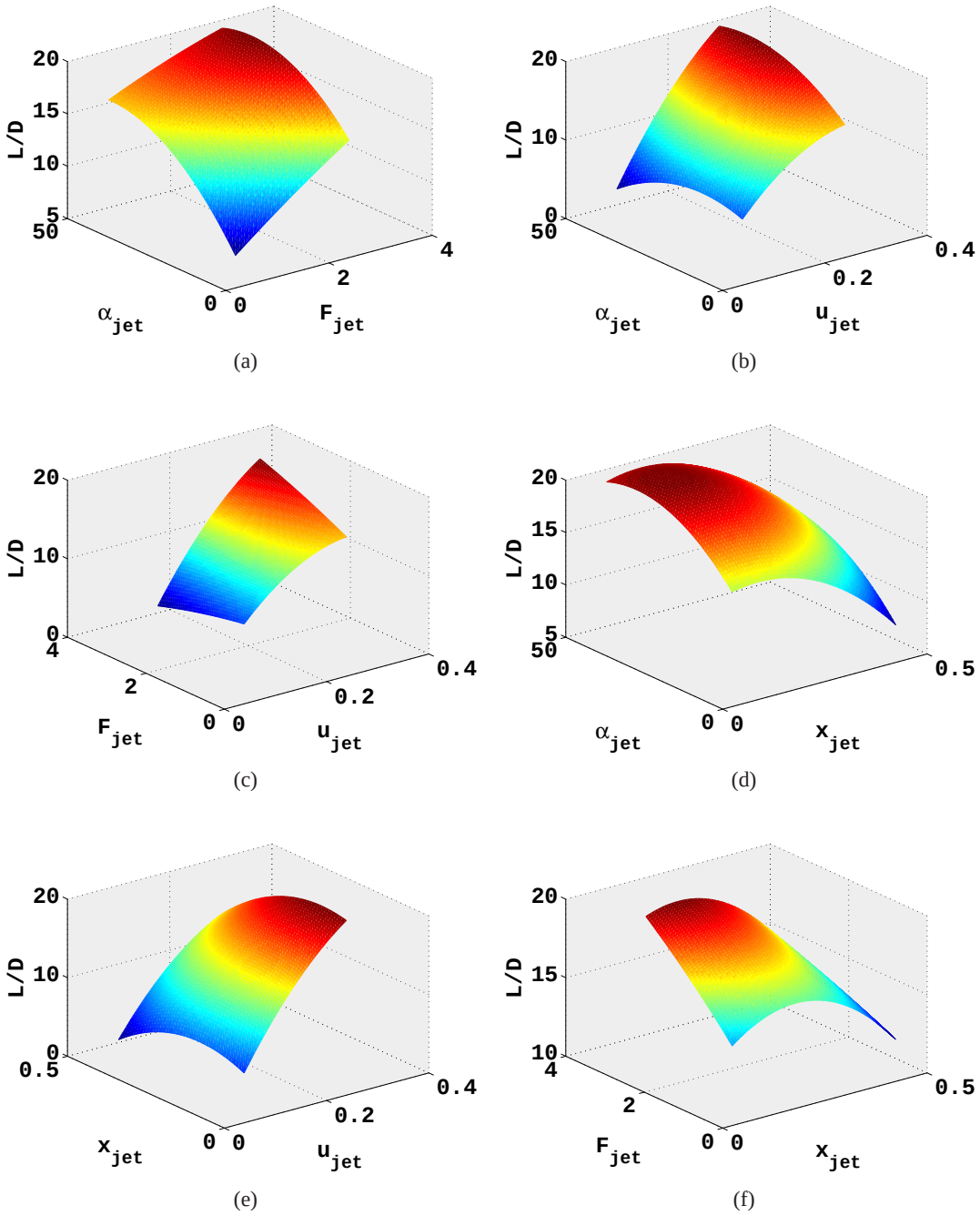

Figure 5.39: Response surfaces at 1st optimization step at α = 18°

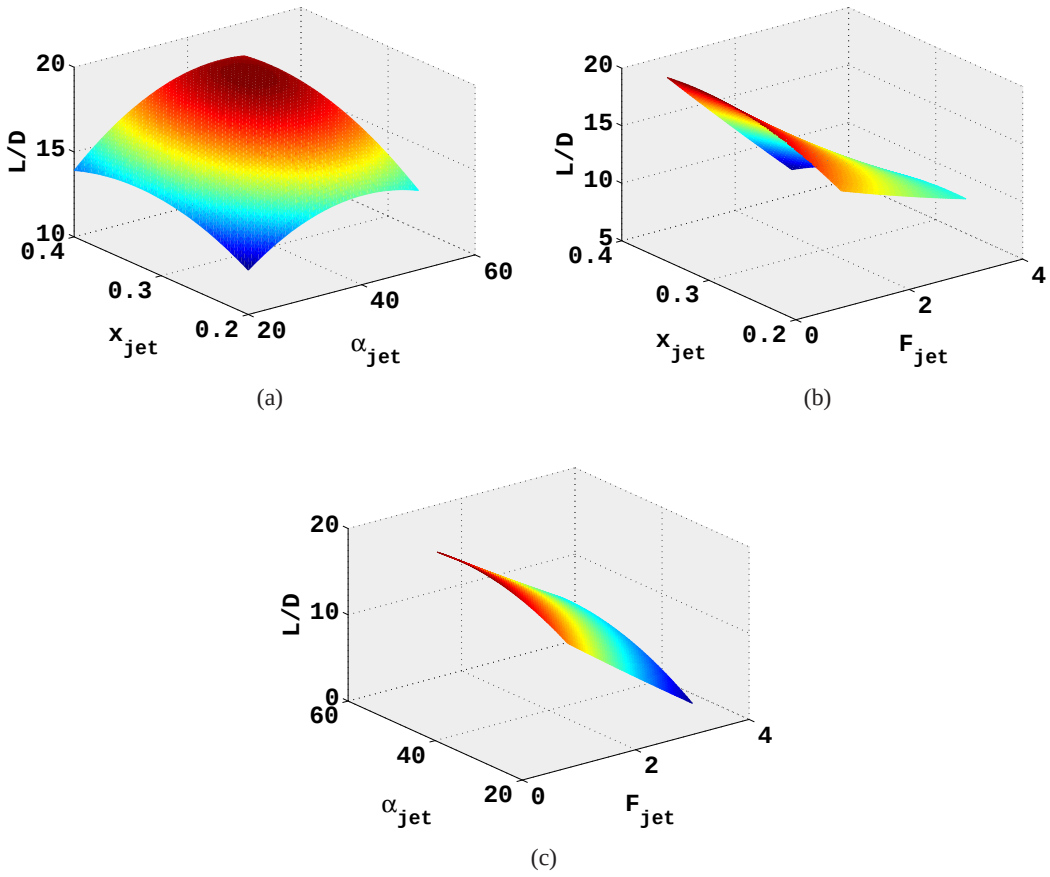

Figure 5.40: Response surfaces at the 3^{rd} optimization step at $\alpha = 18°$

Table 5.11: Aerodynamic coefficients at $\alpha = 18°$

	C_l	C_d	L/D
No jet	0.87	0.15	5.9
With jet	1.33	0.077	18.2
Change(%)	52.6	-51.0	211

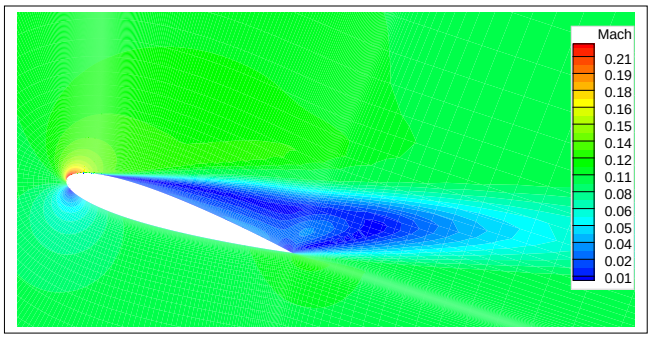

(a) No jet

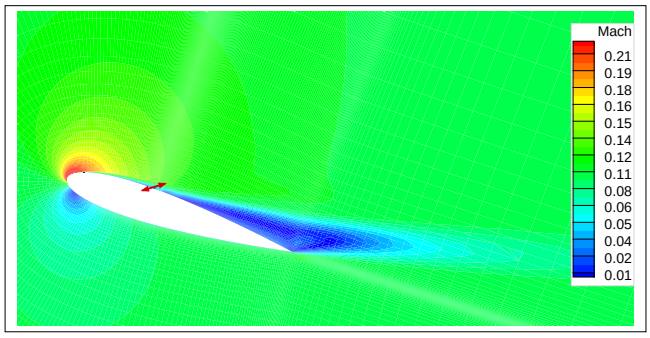

(b) With jet

Figure 5.41: Average streamline patterns at $\alpha = 18°$

attack. The variations of the lift coefficient, drag coefficient, L/D and point of separation with angle of attack are given in Figure 5.45. The lift and drag coefficients are compared before the jet application, after the jet application with initial and optimal jet parameters. It is seen from Figure 5.45(a) that the lift coefficient increases when the synthetic jet is applied, however lift increments were noted when the synthetic jet is applied with optimal parameters. The stall angle of attack is also delayed with the jet actuation. The variation of drag coefficient with angle of attack is shown in Figure 5.45(b). It is observed that drag coefficient is reduced significantly at $\alpha = 18°$. The L/D variation shown in Figure 5.45(c) reveals that the L/D curve shifts upwards with the jet actuation. The increment in L/D is significantly higher for the optimal jet parameters as expected.

The separation point locations with varying angle of attack before and after the synthetic jet application are given in Figure 5.45(d). It is noted that the application of the synthetic jet delays the flow separation at all angles of attack. The synthetic jet is observed to be least effective at $\alpha = 10°$.

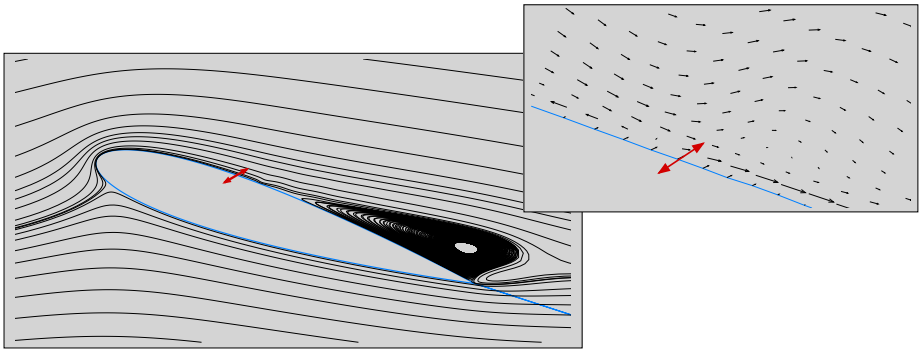

(a) ϕ=0

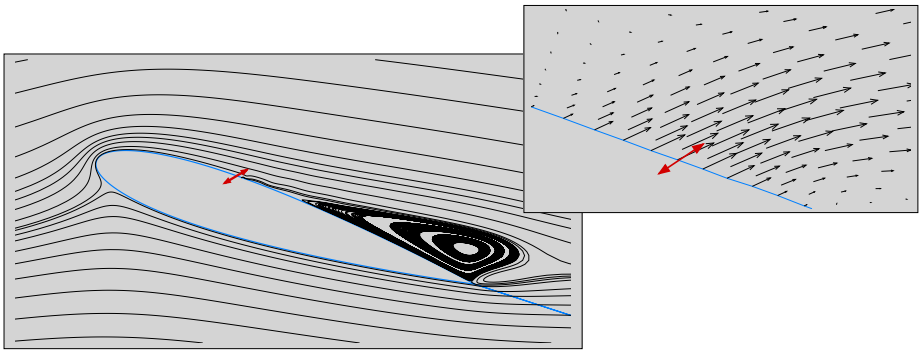

(b) ϕ=π/2

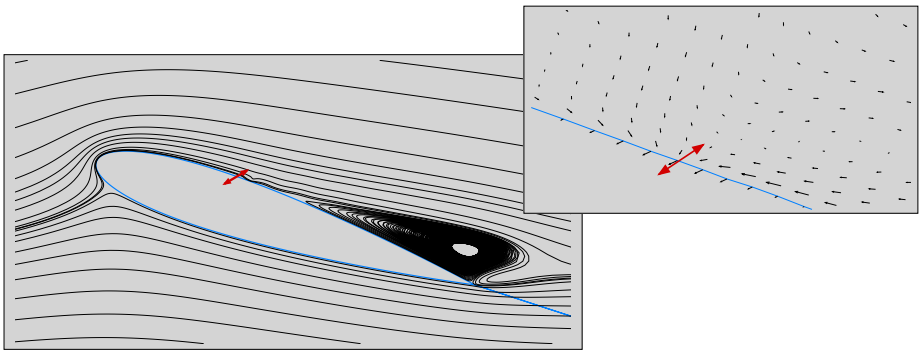

(c) ϕ=π

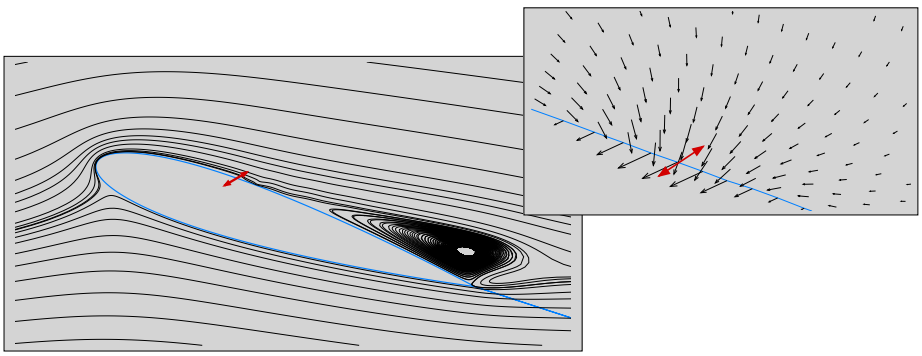

(d) ϕ=3π/2

Figure 5.42: The unsteady flowfield at $\alpha = 18°$

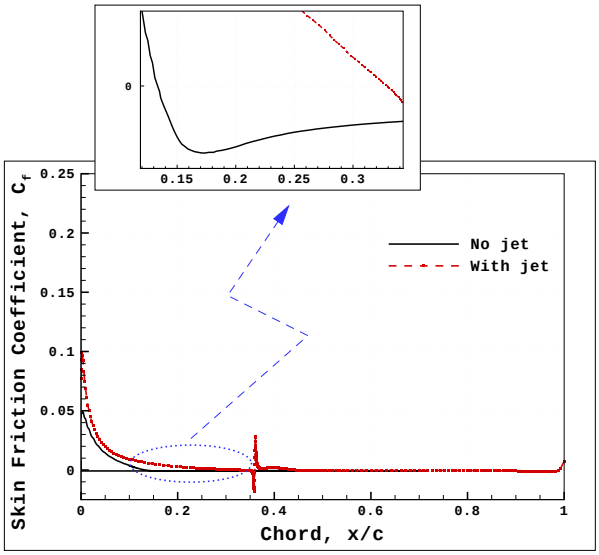

Figure 5.43: Instantaneous skin friction coefficients for the upper surface at $\alpha = 18°$

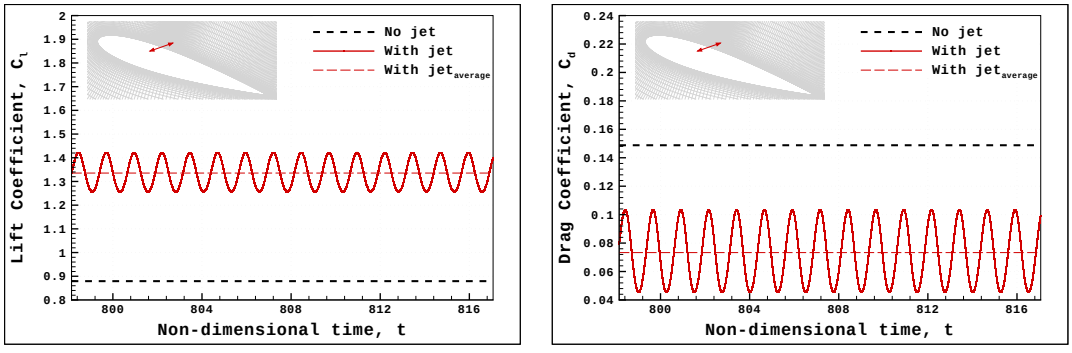

(a) Lift coefficient history

(b) Drag coefficient history

Figure 5.44: Lift and drag coefficient histories at $\alpha = 18°$

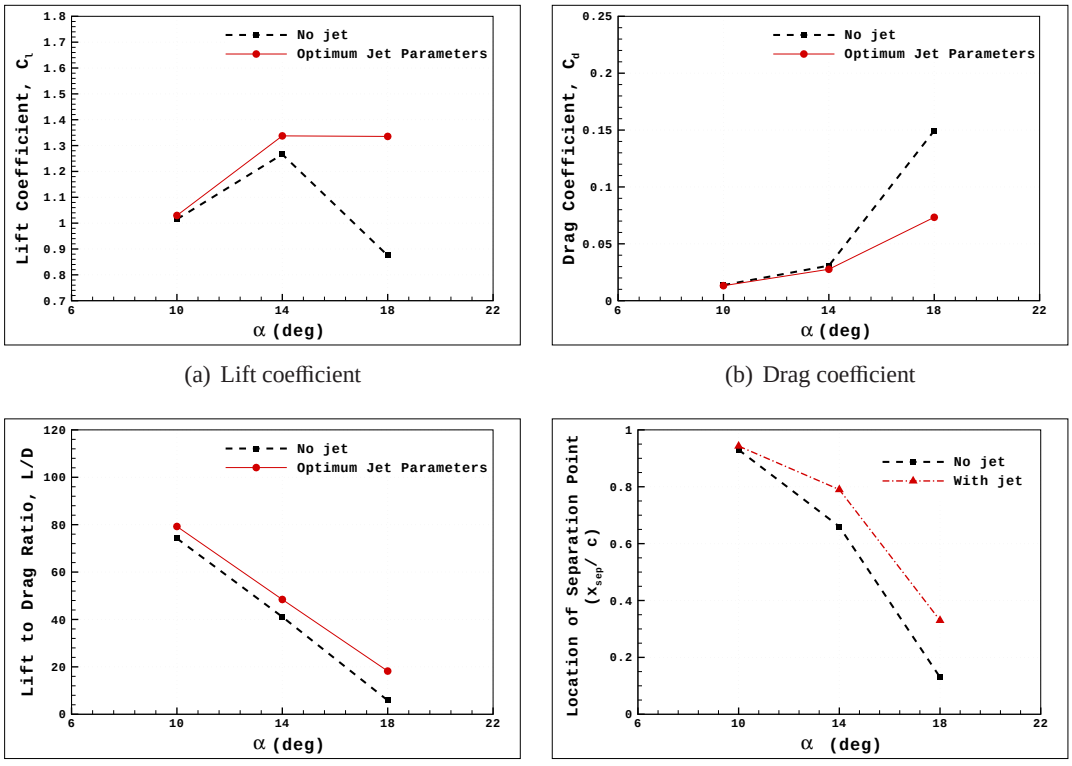

(a) Lift coefficient

(b) Drag coefficient

(c) L/D

(d) Separation point location

Figure 5.45: Results of the optimization study

To summarize the optimization study, the optimization of the synthetic jet parameters is observed to be increasing the synthetic jet performance. The variation of the aerodynamic coefficients with angle of attack (Figure 5.45) proved that the aerodynamic performance of the NACA 0015 airfoil increases significantly especially at high angles of attack when the synthetic jet is applied with the optimum synthetic jet parameters. The variations of the aerodynamic coefficients and the separation point location with the application of the synthetic jet prove that synthetic jets are more effective at high angles of attack.

CHAPTER 6

CONCLUDING REMARKS

The Active Flow Control using a synthetic jet over a NACA 0015 airfoil is successfully studied. The influence of the synthetic jet parameters, the jet velocity, the jet location, the jet angle and the jet frequency are first studied parametrically. The synthetic jet parameters then optimized to maximize the L/D.

Unsteady turbulent flows over the NACA 0015 airfoil are computed using a Navier-Stokes solver. Computations are performed in parallel using PVM library routines in a computer cluster. The Response Surface Methodology, RSM is used in the optimization of the synthetic jet parameters. The optimization studies are carried out at various angles of attack. The computational results are investigated by examining the instantaneous and phase averaged flowfields, load variations in time and the separation point location.

Effect of grid density is first investigated in the circumferential and normal directions and optimum grid sizes in both directions are determined. The validation study is carried out together with the grid sensitivity study. The optimum grid size is used in the solution of the unsteady flowfields at $\alpha = 18°$ and $\alpha = 25°$. The computationally obtained flowfields are then compared with the experimental flowfields. It is observed that the separation point location is predicted well however the flow separation at the leading edge is not predicted accurately in the computational study which may be attributed to the fully turbulent flow assumption.

In parametric studies, the sensitivity of the synthetic jet parameters on the L/D is investigated. The synthetic jet parameters are varied in a wide range and the most effective jet parameters are observed to be the synthetic jet velocity and the jet location. The effectiveness of the synthetic jet observed to be increasing with increasing the jet velocity. The variation of the synthetic jet location is observed to be ineffective on L/D when the synthetic jet is located

far downstream of the separation point. The synthetic jet frequency is found to be a weak parameter in the defined operation range.

Box-Behnken and Full-Factorial design of experiment approaches are employed to approximate the response surfaces for the L/D. It is observed that the two approaches estimate optimum points that are close to each other. The error in the response estimated by the Full-Factorial design is observed to be smaller than the error in the response estimated by the Box-Behnken design. The fact that the Full-Factorial design requires more computational evaluations in approximating the response surfaces is though to be the reason of estimating the response with a better accuracy.

The optimization study is performed for an angle of attack range in which mildly to massively flow separation is observed. The optimization study is performed for a constant power coefficient. The jet slot size is used as a dependent parameter. The synthetic jet parameters used in the optimization study are the jet velocity, the jet location, the jet angle and the jet frequency. The Response Surface Methodology, RSM is used in the optimization of the synthetic jet parameters. The response surfaces are approximated based on the results of the Navier-Stokes solutions for the unsteady, turbulent flows around airfoil. Once the response surface is determined, the maximum value of the response and the corresponding values of the optimization variables are evaluated.

The optimization study shows that the optimum synthetic jet velocity is always the maximum value in the design space at all angles of attack. The optimum synthetic jet angle is observed to be increasing as the angle of attack increases. The optimum synthetic jet location and the location of separation point are observed to be moving through the leading edge as the angle of attack increases from 14° to 18 °. The optimum synthetic jet frequency is observed to the minimum value in the design space at all angles of attack. It should be noted that a smaller jet frequency corresponds to a larger jet slot size for a constant jet power coefficient. As expected, the synthetic jet is shown to be the most effective at post-stall angles of attack. It enhances the L/D significantly and delays the flow separation for separated flows.

REFERENCES

[1] Lee, C. and Goldstein, D., "Two-dimensional synthetic jet simulation." *AIAA Journal*, Vol. 40, No. 3, 2002, pp. 510–516.

[2] Traub, L., Miller, A., and Rediniotis, O., "Effects of Synthetic Jet Actuation on a Ramping NACA 0015 Airfoil," *Journal of Aircraft*, Vol. 41, No. 5, 2004, pp. 1153–1162.

[3] Martin, P., Tung, C., Chandrasekhara, M., and Arad, E., "Active Separation Control: Measurements and Computations for a NACA 0036 Airfoil," *21 st AIAA Applied Aerodynamics Conference*, 2003.

[4] Renault, "Renault Altica: 44MPG Diesel Concept with Active Airflow Management," 2006, http://www.greencarcongress.com/2006/02/renault_altica_.html.

[5] Chen, F. and Beeler, G., "Virtual Shaping of a Two-Dimensional NACA 0015 Airfoil Using Synthetic Jet Actuator," *AIAA Paper*, Vol. 3273, No. 1, 2002.

[6] Gad-el Hak, M., "Modern developments in flow control," *Appl. Mech. Rev*, Vol. 49, No. 7, 1996, pp. 365–379.

[7] Gad-el Hak, M., "Flow Control: The Future," *Journal of Aircraft*, Vol. 38, No. 3, 2001, pp. 401.

[8] Kitsios, V., Kotapati, R., Mittal, R., Ooi, A., Soria, J., and You, D., "Numerical simulation of lift enhancement on a NACA 0015 airfoil using ZNMF jets," *Proceedings of the Summer Program*, 2006, pp. 457.

[9] Schlichting, H. and Gersten, K., *Boundary-Layer Theory*, Springer, 2000.

[10] Seifert, A., Darabi, A., and Wygnanski, I., "Delay of Airfoil Stall by Periodic Excitation," *Journal of Aircraft*, Vol. 33, No. 4, 1996, pp. 691–698.

[11] Duvigneau, R. and Visonneau, M., "Simulation and Optimization of Aerodynamic Stall Control using a Synthetic Jet," *2 nd AIAA Flow Control Conference*, 2004.

[12] Duvigneau, R. and Visonneau, M., "Optimization of a synthetic jet actuator for aerodynamic stall control," *Computers and Fluids*, Vol. 35, No. 6, 2006, pp. 624–638.

[13] Donovan, J., Krai, L., and Cary, A., "Active Flow Control Applied to an Airfoil," *AIAA PaperNo*, 1998, pp. 98–0210.

[14] Patel, M., Kolacinski, R., Prince, T., Ng, T., and Cain, A., "Flow Control Using Intelligent Control Modules for Virtual Aerodynamic Shaping," *AIAA Paper*, Vol. 3663, 2003.

[15] Mallinson, S., Hong, G., and Reizes, J. A., "Fundamental Studies of a Synthetic Jet Actuator," *University of Technology Sydney, 13th Australian Fluid Mechanics Conference*, 1998.

[16] Glezer, A. and Amitay, M., "Synthetic Jets," *Annual Review of Fluid Mechanics*, Vol. 34, No. 1, 2002, pp. 503–529.

[17] Vadillo, J., *Numerical Study of Virtual Aerodynamic Shape Modification of an Airfoil Using a Synthetic Jet Actuator*, Ph.D. thesis, Washington University, 2002.

[18] El-Mistikawy, T., "Separation prevention as an indirect problem based on the triple-deck theory," *AIAA Journal*, Vol. 32, No. 7, 1994, pp. 1423–1427.

[19] Seifert, A., Theofilis, V., and Joslin, R., "Issues in active flow control-Theory, simulation and experiment," *& Proceedings*, 2002.

[20] Gilarranz, J., Traub, L., and Rediniotis, O., "A New Class of Synthetic Jet Actuators-Part II: Application to Flow Separation Control," *Journal of Fluids Engineering(Transactions of the ASME)*, Vol. 127, No. 2, 2005, pp. 377–387.

[21] Bales, K., Khoo, P., and Jefferies, R., "Flow Control of a NACA 0015 Airfoil Using a Chordwise Array of Synthetic Jets," *41 st AIAA Aerospace Sciences Meeting & Exhibit, Reno, NV*, 2003.

[22] Huang, L., Huang, P., LeBeau, R., and Hauser, T., "Numerical Study of Blowing and Suction Control Mechanism on NACA 0012 Airfoil," *Journal of Aircraft*, Vol. 41, No. 5, 2004, pp. 1005–1013.

[23] Utturkar, Y., Holman, R., Mittal, R., Carroll, B., Sheplak, M., and Cattafesta, L., "A Jet Formation Criterion for Synthetic Jet Actuators," *AIAA Paper*, Vol. 636, 2003, pp. 2003.

[24] Smith, B., "The formation and evolution of synthetic jets," *Physics of Fluids*, Vol. 10, No. 9, 1998, pp. 2281.

[25] Hamdani, H., Baig, A., and Zahir, S., "A Systematic Study of Separation Control by Varying Various Parameters During Alternating Tangential Blowing/Suction," *AIAA paper*, Vol. 422, 2003.

[26] Parekh, D., Glezer, A., Allen, M., Crittenden, T., and Birdsell, E., *AVIA: Adaptive Virtual Aerosurface*, Defense Technical Information Center, 2004.

[27] Wang, Z. and Stoffel, B., "Behavior of synthetic jet on stalled airfoil flow," *AIAA Paper*, Vol. 222, 2003.

[28] Kaya, M. and Tuncer, I. H., "Response Surface Method for the Maximization of Thrust in Flapping Airfoils,AIAC-2007-011," *4th Ankara International Aerospace Conference*, 2007.

[29] Akçayöz, E., Erler, E., and Tuncer, I. H., "Flow Control Studies Over an Airfoil and an Elliptic Profile,AIAC-2007-120," *4th Ankara International Aerospace Conference*, 2007.

[30] Kaya, M., *Computation of Viscous Flows Over Flapping Airfoils and Parallel Optimization of Flapping Parameters*, Master's thesis, METU, 2003.

[31] Hoffmann, K. A. and Chiang, S. T., "Computational Fluid Dynamics Volume III," *Engineering Education System, Wichita, Kansas*, 2000, pp. 48–50.

[32] Lin, C., Ecer, A., Satofuka, N., Fox, P., and Periaux, J., editors, *Parallel computational fluid dynamics : Development and Applications of Parallel Technology*, Elsevier, 1999.

[33] Geist, A., Beguelin, A., Dongarra, J., Jiang, W., Manchek, R., and Sunderam, V., "PVM 3 User's Guide and Reference Manual," *Oak Ridge National Laboratory, Oak Ridge, Tennessee*, Vol. 37831, 1994.

[34] Kowalik, J., editor, *PVM: Parallel Virtual Machine A Users' Guide and Tutorial for Networked Parallel Computing*, The MIT Press Cambridge, Massachusetts, 1994.

[35] Blazek, J., "Computational Fluid Dynamics: Principles and Applications,2001," , pp. 267–276.

[36] Montgomery, D., "Design and Analysis of Experiments," *New York*, 1991, pp. 542–546,521–523.

[37] Khuri, A. I. and Cornell, J. A., *Response Surfaces Design and Analyses*, Vol. 81, ASQC Quality Press, 1987.

[38] Myers, R., *Response Surface Methodology*, Allyn and Bacon, Inc., Boston, 1971.

[39] Mavris, D., "Introduction to Design of Experiments and Response Surface," Presentation, 2007.

[40] Tuck, A. and Soria, J., "Active Flow Control over a NACA 0015 Airfoil Using a ZNMF Jet,'," *15 thAustralasian Fluid Mechanics Conference, Sydney, Australia, Univ. of Sydney Paper*, Vol. 178, 2004, pp. 13–17.

[41] Hassan, A., "Numerical Simulations and Potential Applications of Zero-Mass Jets for Enhanced Rotorcraft Aerodynamic Performance," *AIAA Paper*, 1998, pp. 98–0211.